Statistical Interpretation of Exotics Monojet Data In Search Of An Invisibly Decaying Higgs Boson

Chilufya Mwewa
Department of Physics, University Of Cape Town (UCT)

Supervised by: Dr Andrew Hamilton

11 April, 2014

Submitted in fulfillment of the requirements for a Master of Science degree

Submitted in fulfilment of the requirements for a Master of Science Degree in the Department of Physics at the University of CapeTown

Chilufya Mwewa

mwwchi001@myuct.ac.za

This dissertation is submitted to the Faculty of Science at the University of CapeTown, in partial fulfilment of the requirements for the degree of Master in Science.

As the candidate's supervisor, I have approved this dissertation for submission.

Signed: Dr Andrew Hamilton .....

Student Declaration

I, the undersigned, hereby declare that the work contained in this thesis is my original work, and that any work done by others previously has been acknowledged and referenced accordingly.

Signed by candidate

Chilufya Mwewa, 11 April 2014

Abstract

Following the recent discovery of a Standard Model Higgs-like particle at the Large Hadron Collider, this study searches for the evidence of invisible decays of this particle. Assuming that this is the Standard Model Higgs boson, its decay to invisible particles is not expected to be measurable in the current data. However, it could have a large contribution from its decay to stable non-Standard Model particles such as the hypothetical dark matter particles. This study corresponds to 4.7 fb^{-1} of 7 TeV proton-proton collisions and 20.3 fb^{-1} of 8 TeV proton-proton collisions. At the time of thesis submission, the 8 TeV results were not unblinded by the ATLAS Collaboration, so toy-data are presented here to demonstrate the procedure. The performance of the statistical framework to be used in the combination of the 7 TeV data with the real 8 TeV data is assessed and is found to perform very well. The results are interpreted to set 95$\%$ confidence level limits on the branching ratio to invisible particles of the newly discovered Higgs-like particle at a mass of 125 GeV. Limits are also set on the production cross section $\times$ branching ratio of additional Higgs-like particles that decay invisibly in the mass range: 115 GeV to 300 GeV. In the combination of the 7 TeV data and 8 TeV toy-data, an expected (observed) upper limit of 0.89 (0.59) is set on the branching ratio to invisible particles of a 125 GeV Higgs boson. In the mass range 115 to 300 GeV, no excess beyond the Standard Model expectation is observed.

Acknowledgements

I wish to express my sincere gratitude to the various indivividuals and groups that made the success of this thesis possible and groomed me into becoming a better researcher. I am positive that the lessons I have learned throughout this research have taken me to a much greater level in my career than I was and with the skills obtained, I will go even higher.

Firstly, I would like to offer my deepest gratitude to my research superviser Dr Andrew Hamilton for the patient and professional guidance he offered to this research. I also thank him for his enthusiastic encouragement and extremely useful critiques of this research. I extend special thanks to Prof Ketevi Adikle Assamagan and Dr German Montoya Carrillo for their consistent advice and assistance in keeping my progress on schedule and for giving an ear to even the most naive questions I had. Furthermore I greatly appreciate them for teaching me the necessary skills required in the analysis part of this research.

I also thank the monojet group at the LHC's ATLAS experiment for allowing me to work within their collaboration and to use their data for the purpose of this research. I additionally wish to show my deep appreciation for the SA-CERN collaboration for funding my research visit to the ATLAS experiment. I am grateful to the staff of the African Institute for Mathematical Sciences (AIMS) and the University of Cape Town (UCT) post graduate funding office for funding my studies.

Finally, I wish to thank my mother Ms Gladys Mushinge and my young sister Ms Mariana Mwewa for their loving support and encouragement throughout my studies. I also thank my dear family and friends for their care and support throughout my studies. A special acknowledgement to Ms Claire Antel for taking her time to read through my thesis and for her valuable comments.

To my loving fiance Mr David Kapya, words can not express how grateful I am for the care, support, positive rebukes and encouragement you have given me so far in my postgraduate studies. I value the lessons you teach me everyday and am in awe of your love. God Bless you always!

Contents

Abstract ii

Acknowledgements iii

Introduction 1

1 Theoretical Background 3
- 1.1 The Standard Model . . . 3

2 The LHC and the ATLAS Detector 9
- 2.1 The Large Hadron Collider . . . 9
- 2.2 The ATLAS Detector . . . 11
- 2.3 Particle Reconstruction and Identification . . . 13

3 The Search For The Higgs Boson 20
- 3.1 Statistical Methods For Particle Physics Analysis . . . 20
- 3.2 Results From Earlier Experiments . . . 25
- 3.3 Search for the Higgs Boson at ATLAS . . . 26
- 3.4 Search for an Invisibly Decaying Higgs Boson . . . 28

4 Methodology 30
- 4.1 Data Inputs at 7 and 8 TeV . . . 31
- 4.2 Implementation of Statistical Techniques . . . 34

5 Results 36
- 5.1 Results at 7 TeV . . . 36
- 5.2 Results at 8 TeV 1-jet category . . . 40
- 5.3 Results at 8 TeV 2-jet category . . . 43
- 5.4 Combined 7 TeV and 8 TeV Results . . . 46

Conclusion 48

Bibliography **53**

A **54**

List of Tables

2.1 Pseudorapidity coverage of the ATLAS sub-detectors [Dan98]. 13

4.1 Definition of the 7 TeV signal regions. 32
4.2 Definition of the 8 TeV 1−jet signal regions. 32
4.3 Definition of the 8 TeV 2−jet signal regions. 32
4.4 Acceptance×Efficiency used for the 125 GeV Higgs in SR1 (7 TeV). 32
4.5 Production Cross sections for a 125 GeV Higgs at 7 TeV. The uncertainties shown represent QCD effects (first) and PDF (Parton distribution function) effects (second). 33
4.6 Number of observed data events and expected background events with their statistical uncertainties in SR1 (7 TeV) at 125 GeV 34
4.7 Theoretical and detector systematic uncertainties in SR1 (7 TeV) at 125 GeV . . 35

5.1 SR1 Limits at all mass points at 7 TeV 37
5.2 SR2 Limits 37
5.3 SR3 Limits 37
5.4 SR4 Limits 38
5.5 SR1 Limits at all mass points at 8 TeV 1-jet 40
5.6 SR3 Limits at 8 TeV 1-jet 40
5.7 SR5 Limits at 8 TeV 1-jet 41
5.8 SR1 Limits at all mass points at 8 TeV 2-jet 43
5.9 SR3 Limits at 8TeV 2-jet 43
5.10 SR5 Limits at 8TeV 2-jet 44
5.11 Combined 7 and 8 TeV Limits 46

List of Figures

1.1 Standard Model particles [Std14] . . . 4
1.2 Interactions of fundamental Standard Model particles [Std14] . . . 4
1.3 Illustration of the Higgs potential as a function of two of its componets (ϕ_1 and ϕ_2) [Mos11]. . . . 7

2.1 The Large Hadron Collider [Mos11] . . . 10
2.2 The ATLAS detector [Col08b]. . . . 11
2.3 ATLAS Coordinate System. . . . 13
2.4 Particle Identification [Vir12]. . . . 14
2.5 (a) Event display of a reconstructed electron from a candidate W decay. The electron cluster is shown in yellow, in the green electromagnetic calorimeter [Ali12]. (b) Event display of a reconstructed diphoton pair. The photon clusters are shown in yellow in the green electromagnetic calorimeter [Col12b]. In both pictures, the blue lines represent inner detector tracks and the red dotted lines in (a) represent E_T^{miss}. . . . 16
2.6 (a) Event display of a reconstructed jet in the transverse plane [col13b] of the ATLAS detector. (b) Event display of reconstructed missing transverse energy in the ATLAS detector [Col11a]. . . . 17

3.1 Example: The observed and expected 95% confidence level limits on μ for the combined search of the Higgs boson for the period 2011-2012 [Col12a]. . . . 24
3.2 A lower limit of $114.4\mathrm{GeV}$ set on the Higgs mass by LEP experiments [Sea03]. . 25
3.3 Feynmann diagrams of Higgs production modes. Gluon fusion (a), vector boson fusion (b),associative production with W/Z (c) and associative production with a top pair (d) [Ege98] . . . 27
3.4 (a) Higgs production cross sections as a function of mass at 8 TeV center of mass energies. (b) Higgs decay branching ratios as a function of mass. [cswg13] . . . 27
3.5 The observed (solid) local pvalue (p_0) as a function of m_H in the low mass range. The dashed curve shows the expected local pvalue under the hypothesis of a SM Higgs boson signal at that mass [Col12a]. . . . 28

3.6 (a) Confidence level (CL) scanned against BR(H→invisible) for the SM Higgs boson at 125 GeV. (b) 95% confidence level limits on the cross section times branching ratio of a Higgs-like particle decaying to invisible particles [Col13d]. . . 29

5.1 Observed and expected confidence level limits on the ($\sigma\times$BR(H $\rightarrow$ invisible)/σ_{SM}) of a 125 GeV Higgs boson in the 7 TeV category for all signal regions considered. The blue solid line indicates a 1-68%CL and the red solid line indicates a 1-95%CL. 38

5.2 95%CL upper limits on the cross section$\times$branching ratio of a Higgs-like particle decaying to invisible particles in the mass range 115 to 300 GeV at $\sqrt{s}$ =7 TeV. 39

5.3 [$\sqrt{s}$ =8 TeV (1-jet category)] Left panel: Observed and expected confidence level limits on the ($\sigma\times$BR(H $\rightarrow$ invisible)/σ_{SM}) of a 125 GeV Higgs boson. The blue solid line indicates 1-68%CL and the red solid line indicates 1-95%CL. Right panel: 95%CL upper limits on the cross section$\times$branching ratio of a Higgs-like particle decaying to invisible particles in the mass range 115 to 300 GeV. 42

5.4 [$\sqrt{s}$ =8 TeV (2-jet category)] Left panel: Observed and expected confidence level limits on the ($\sigma\times$BR(H $\rightarrow$ invisible)/σ_{SM}) of a 125 GeV Higgs boson. The blue solid line indicates 1-68%CL and the red solid line indicates 1-95%CL. Right panel: 95%CL upper limits on the cross section$\times$branching ratio of a Higgs-like particle decaying to invisible particles in the mass range 115 to 300 GeV. 45

5.5 The observed and expected 95% confidence level limits on on the Branching ratio for the combined search of an invisibly decaying 125 GeV Higgs. 46

5.6 The observed and expected 95% confidence level limits on the cross section $\times$ Branching ratio for the combined search of an invisibly decaying Higgs-like particle in the mass range 115 GeV to 300 GeV. 47

Introduction

The Standard Model of particle physics is considered one of the most successful theories in physics; it provides a unified description of the fundamental constituents of matter and their interactions. Within the Standard Model, the origin of particle masses is the Higgs field, which is mediated by a scalar boson called the Higgs boson [F.E64], [W.H64].

Since its prediction in 1964, various experiments have searched for the Standard Model (SM) Higgs boson. The primary goal of the Large Hadron Collider (LHC) at the European Center for Nuclear Research (CERN), was to search for the SM Higgs boson [Col99]. In July, 2012, a new particle consistent with the SM Higgs boson was observed by the ATLAS and CMS experiments at CERN at a mass of about 125 GeV [Col12a], [Col12f]. The discovery was established by observing the decay of the SM Higgs boson in the following channels; diphoton ($\gamma\gamma$), $\mathrm{ZZ} \rightarrow 4l$ and $\mathrm{WW} \rightarrow e\nu\mu\nu/\mu\nu e\nu$. The combined search for the SM Higgs boson in these channels gave statistically significant excess of events, indicating the existence of a SM Higgs boson. Studies have since been conducted to check the compatibility of this new particle's properties with the SM Higgs boson and each study has shown consistency with the SM Higgs boson [Col13f],[Col13e]. These studies also include searching for other decay channels predicted by the Standard Model, in which the Higgs has not yet been observed.

This study explores one of these decay channels; the "invisible" channel, in which the Higgs decays to unseen particles that can only be detected as missing transverse energy. Results obtained in previous searches have not excluded the possibility of a sizable branching ratio of the SM Higgs to invisible particles [Col13a]. A further Higgs-like particle decaying exclusively to invisible particles is also not excluded for $\mathrm{m_H}$ >115 GeV [Col13g], [Col13c]. The main focus of this study is to set limits on the branching ratio of the SM Higgs at 125 GeV in the invisible decay channel in the absence of a statistically significant observed signal. In addition, limits are set on the cross section $\times$ branching ratio of additional Higgs-like particles that decay invisibly in the mass range: 115 to 300 GeV. The data used includes events with one or two jets plus missing transverse energy. Statistical techniques used for limit setting are employed and form the main component of this thesis.

This thesis is organised as follows. Chapter 1 gives an overview of the Standard Model and the Higgs mechanism. Chapter 2 describes the structure of the LHC and the ATLAS detector. Chapter 3 gives an account of the experiments conducted in search of the SM Higgs boson. In addition, the statistical methods used by ATLAS for establishing discovery, parameter fitting and setting limits are highlighted. Chapter 4 explains the procedure followed in obtaining the data

used in this study and the statistical methods used to analyse it. Chapter 5 presents the results obtained and finally, Chapter 5.4 discusses and draws conclusions on these results.

1. Theoretical Background

The goal of particle physics is to explain the fundamental make up of nature to as basic a level as possible. The Standard Model is able to explain, to a very large extent, all matter particles and the forces that are responsible for their interactions [ea03a]. It also explains the origin of their masses via the Higgs mechanism, a mechanism responsible for electroweak symmetry breaking.

This chapter gives some theoretical background behind the Standard Model and the Higgs mechanism. Section 1.1 briefly describes the Standard Model. Subsections 1.1.1 and 1.1.2 focus on the electroweak theory and the Higgs mechanism respectively.

1.1 The Standard Model

The Standard Model classifies fundamental particles as fermions (spin $\frac{1}{2}$) and bosons (spin 0 or 1) [M.K01]. Fermions are subdivided into quarks and leptons, which are further categorized into three different generations as shown in Fig. 1.1. Other than their masses increasing from the first to the third generation, the particles of each generation possess similar properties. Our everyday life is made up of the first generation fermions which are the lightest and are hence stable. These include the up quark, the down quark and the electron. In addition, neutrinos are also readily available in nature. Each fermion also has a corresponding antiparticle which is identical to it in mass and spin but with opposite electric charge. However, both neutrinos and antineutrinos are electrically neutral and whether or not the two are identical particles is yet to be verified [Need reference].

Also shown in Fig. 1.1 are the gauge bosons as well as the scalar (spin 0) Higgs boson. Gauge bosons, also known as vector bosons (spin 1), are the force mediators and are responsible for fermion interactions. Each gauge boson is responsible for at least one type of interaction among the strong, electromagnetic and weak interactions. The strong interactions are mediated by gluons and are explained by a quantum field theory[1] known as Quantum Chromodynamics (QCD). Particles interacting via the strong force exchange gluons between them. For example, quarks in a proton are held together as a result of gluon exchange between them. The strong force is the most dominant of all the forces, however, it has a very short range and can only be observed at atomic distances. QCD also introduces the concept of a color charge which is analogous to

[1] A quantum field theory is a theoretical framework that combines the fundamental and relativistic aspect of elementary particles to construct quantum mechanical models of the interaction of physical fields with matter.

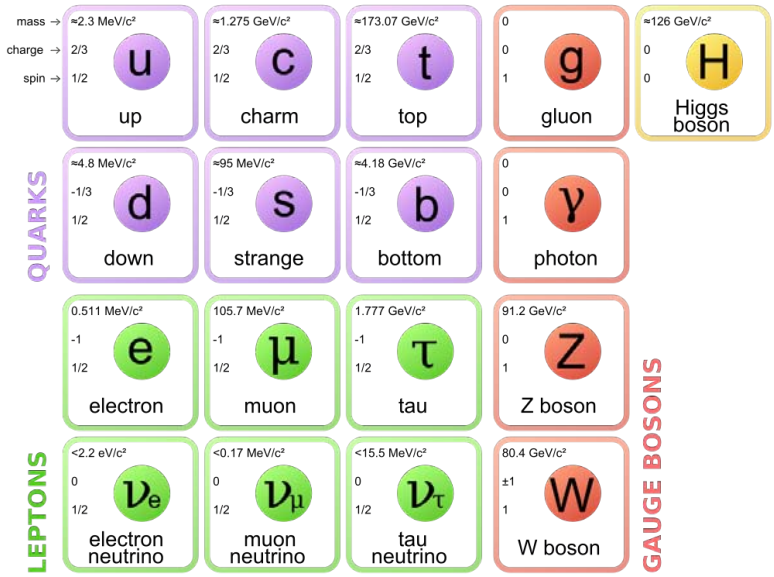

Figure 1.1: Standard Model particles [Std14]

the electric charge in electromagnetic interactions. In this case, a quark can either carry a color charge of red, green or blue. Gluons also posses color charge but with a combination of two colors, hence they interact with eachother. Leptons do not carry a color charge and hence they do not interact via the strong interaction. Electromagnetic interactions are mediated by photons and are explained by a quantum field theory known as Quantum Electrodynamics (QED). Particles interacting electromagnetically must posses an electric charge. Unlike gluons, photons do not carry an electric charge and hence they do not directly interact with each other. Finally, the weak interactions are mediated by the W and Z bosons. Other than the gluon, all elementary particles interact via the weak interactions. Fig. 1.2 shows a summary of all possible elementary particle interactions in the Standard Model.

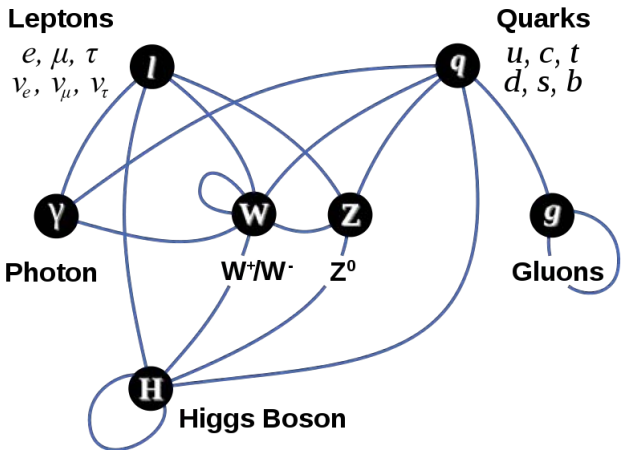

Figure 1.2: Interactions of fundamental Standard Model particles [Std14]

In quantum field theory, the interactions of physical fields with matter are explained by the Lagrangian density. Requiring the Lagrangian density to be invariant under a continuous group of local gauge transformations, known as local gauge invariance, leads to the prediction of massless vector bosons. This is not a problem for QED and QCD which are mediated by massless vector bosons (photons and gluons). However, weak interactions are mediated by the massive W and Z vector bosons, causing difficulty for the theory. To overcome this difficulty, the Standard Model introduces the Higgs mechanism which spontaneously breaks the symmetry of the Lagrangian while giving mass to the W and Z bosons and leaving the photon massless.

Subsection 1.1.1 describes the theoretical formulations of the electroweak theory and the Higgs mechanism. Much of the material used here in explaining these theories is taken from [Gri08], [Bet08], [Man10].

1.1.1 The Electroweak Theory and the Higgs Mechanism. In the Standard Model, gauge transformations are represented as groups whose generators are force carriers of the corresponding interaction. The Standard Model is invariant under the symmetry group given in Equation 1.1.1.

$$\mathrm{SU}(3)_c \times \mathrm{SU}(2)_{I_w} \times \mathrm{U}(1)_{Y_w} \tag{1.1.1}$$

In Equation 1.1.1, the first term represents QCD with the subscript c standing for color. The last two terms together represent the electroweak theory. This involves both charged currents (CC) and neutral currents (NC) of the electromagnetic and weak interactions. Weak CC are mediated by the $\mathrm{W}^{\pm}$ bosons and are represented by the $\mathrm{SU}(2)$ symmetry group. The $\mathrm{U}(1)$ symmetry group represents NC, mediated by the Z^0 boson for the weak sector and the photon for the electromagnetic sector. The subscripts I_w and Y_w represent the quantum numbers; weak isospin and weak hypercharge respectively.

The electroweak theory is a chiral gauge theory, such that it describes left and right-handed fermions. For example, charged weak interactions only act on left-handed particles, whereas the neutral weak interactions involve both chiralities. The charged weak currents are given by Equation 1.1.2, where χ_L represents a left-handed particle doublet and $\tau^{\pm}$ are 2×2 matrices composed of the linear combination of two Pauli matrices. A third weak current, j^3_μ, which ensures a full weak isospin symmetry, is given by Equation 1.1.3.

$$j^{\pm}_\mu = \chi_L \gamma_\mu \tau^{\pm} \chi_L \tag{1.1.2}$$

$$j^3_\mu = \bar{\chi_L} \gamma_\mu \frac{1}{2} \tau^3 \chi_L \tag{1.1.3}$$

The neutral weak current is given by Equation 1.1.4, where $j^{e.m}_\mu$ is the electric current.

$$j^Y_\mu = 2j^{e.m}_\mu - 2j^3_\mu \tag{1.1.4}$$

The weak isospin currents ($j_\mu^\pm$ and j_μ^3) couple, with strength g_w, to a weak isotriplet of vector bosons, $\vec{W}$, whereas the weak hypercharge current couples, with strength $\frac{g\prime}{2}$ to an isosinglet, B . From this, the two neutral states, W^3 and B, mix to produce one massless linear combination (the photon, represented by A_μ) and an orthogonal massive combination (Z^0) according to Equation 1.1.5, where θ_w is the weak mixing angle, experimentally determined to be approximately 29°.

$$\begin{pmatrix} Z_\mu \\ A_\mu \end{pmatrix} = \begin{pmatrix} \cos\theta_w & -\sin\theta_w \\ \sin\theta_w & \cos\theta_w \end{pmatrix} \begin{pmatrix} W_\mu^3 \\ B_\mu \end{pmatrix} \tag{1.1.5}$$

The weak mixing angle also relates the CC and NC coupling constants via Equation 1.1.6. These coupling contants are then related to the electric charge according to Equation 1.1.7.

$$g\prime = g\tan\theta_w \tag{1.1.6}$$

$$g\sin\theta_w = \frac{q_e}{\sqrt{\epsilon_0 \frac{hc}{\sqrt{2}\pi}}} \quad \text{and} \quad g\prime\cos\theta_w = \frac{q_e}{\sqrt{\epsilon_0 \frac{hc}{\sqrt{2}\pi}}} \tag{1.1.7}$$

With the above formulations, the Lagrangian density describing the electroweak theory can be expressed by Equation 1.1.8. The terms in this expression represent the CC weak interactions, NC weak interactions and the electromagnetic interactions, respectively. Hence, the weak and electric charges are unified.

$$\mathcal{L} = \frac{g}{\sqrt{2}}(j_\mu W_+^\mu + j_\mu W_-^\mu) + \frac{g}{\cos(\theta)_w}(j_\mu^3 - \sin^2\theta_w j_\mu^{EM})Z^\mu + g\sin\theta_w j_\mu^{EM} A^\mu \tag{1.1.8}$$

However, the above unification requires the $W^\pm$ bosons, the Z boson and the photon to be massless in order to allow for local gauge invariance. This problem is overcome by the introduction of the Higgs mechanism, in which a Higgs field interacts with the gauge bosons, giving mass to the $W^\pm$ and Z bosons while leaving the photon massless. The Higgs boson acts as the mediator of the Higgs field. The interaction of the Higgs field with the gauge bosons is gauge invariant. However, in the vacuum state[2], the Higgs field has a non-zero value which is non-invariant under a gauge transformation. Hence, in this state, the theory is no longer gauge invariant and the gauge bosons are no longer required to be massless. This is known as spontaneous symmetry breaking. Section 1.1.2 gives a brief and general illustration of spontaneous symmetry breaking in relation to the Higgs mechanism. The reader is referred to [Gri08].

1.1.2 Spontaneous Symmetry Breaking and The Higgs Mechanism. Spontaneous symmetry breaking occurs when some symmetric property of a system is not exhibited in the lowest energy state. In the electroweak sector, spontaneous symmetry breaking occurs when the full

[2]Where no other particles are present

electroweak Lagrangian is required to be locally gauge invariant. Local gauge invariance works well for the electromagnetic interactions since they are mediated by massless photons. However, when applied to the weak interactions, the $W^{\pm}$ and Z bosons are required to be massless. To achieve local gauge invariance, while keeping the $W^{\pm}$ and Z bosons massive, the Higgs field, ϕ with a potential $\mathrm{V}(\phi)$, is introduced, which interacts with the electroweak field. The Higgs potential is shown in Fig. 1.3.

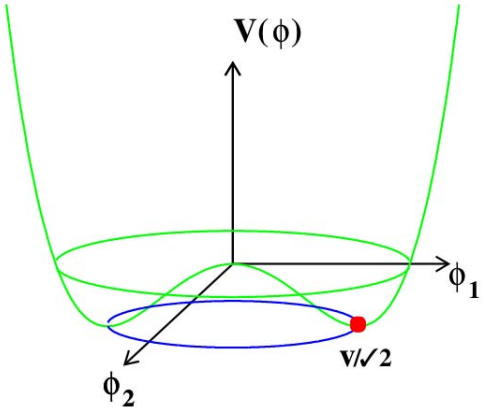

Figure 1.3: Illustration of the Higgs potential as a function of two of its componets (ϕ_1 and ϕ_2) [Mos11].

To illustrate the Higgs mechanism, consider Equation 1.1.9 to be the Lagrangian related to the Higgs field. According to this Lagrangian, the Higgs potential is represented by Equation 1.1.10.

$$\mathcal{L} = \frac{1}{2}(\partial_\mu\phi)^*(\partial^\mu\phi) + \frac{1}{2}\mu^2(\phi^*\phi) - \frac{1}{4}\lambda^2(\phi^*\phi)^2 \tag{1.1.9}$$

$$\mathrm{V}(\phi) = -\frac{1}{2}\mu^2(\phi^*\phi) + \frac{1}{4}\lambda^2(\phi^*\phi)^2 \tag{1.1.10}$$

Under local gauge transformations (i.e $\phi \rightarrow e^{i\theta(x)}\phi$), this Lagrangian can be made locally gauge invariant by introducing a massless gauge field, Q^μ (which in this case is the weak field), and replacing the derivatives by the covariant derivative given by Equation 1.1.11. The Lagrangian then becomes Equation 1.1.12, where $F^{\mu\nu}$ represents the field strength tensor.

$$D_\mu = \partial_\mu + i\frac{q}{\hbar c}\mathrm{Q}_\mu \tag{1.1.11}$$

$$\mathcal{L} = \frac{1}{2}\left[\left(\partial_\mu - \frac{iq}{\hbar c}\mathrm{Q}_\mu\right)\phi^*\right]\left[\left(\partial^\mu + \frac{iq}{\hbar c}\mathrm{Q}^\mu\right)\phi\right] + \frac{1}{2}\mu^2(\phi^*\phi) - \frac{1}{4}\lambda^2(\phi^*\phi)^2 - \frac{1}{16\pi}F^{\mu\nu}F_{\mu\nu} \tag{1.1.12}$$

Following from the idea that Feynman calculus is a perturbative procedure, in which we start from the vacuum state and treat the fields as fluctuations about that state, if we project into the vacuum state of this Lagrangian and look for two minimum points of $V(\phi)$, we find that the field Q^{μ} acquires a mass. Suppose we choose $\phi_{1_{min}} = \frac{\mu}{\lambda}$ and $\phi_{2_{min}} = 0$ and define two new fields, N and M, that fluctuate about these points (i.e $\mathrm{N} = \phi_1 - \frac{\mu}{\lambda}$ and $\mathrm{M} = \phi_2$). The Lagrangian, ignoring the Goldstone boson[3] [JG62], is then given by Equation 1.1.13.

$$\mathcal{L} = \left[\frac{1}{2}(\partial_{\mu}\mathrm{N})(\partial^{\mu}\mathrm{N}) - \mu^2\mathrm{N}^2\right] + \left[-\frac{1}{16\pi}F^{\mu\nu}F_{\mu\nu} + \frac{1}{2}\left(\frac{q}{\hbar c}\frac{\mu}{\lambda}\right)\mathrm{Q}_{\mu}\mathrm{Q}^{\mu}\right] + \ldots \tag{1.1.13}$$

In this locally gauge invariant Lagrangian, the field N is associated with a scalar particle of mass $\sqrt{2}\mu\frac{\hbar}{c}$ and the initially massless gauge field, Q^{μ}, has now acquired a mass given by Equation 1.1.14. In this example, the massive scalar particle associated with the field, N, represents the Higgs boson. Therefore, by interacting with the Higgs field, massless gauge fields acquire mass, hence the mass of the weak mediators.

$$\mathrm{M}_{\mathrm{Q}} = 2\sqrt{\pi}\left(\frac{q\mu}{\lambda c^2}\right) \tag{1.1.14}$$

For many decades, the theory of the Higgs mechanism remained unverified as no experiment managed to observe the Higgs boson. Examples of early experiments involved in this search include ALEPH and DELPHI at LEP as well as CDF and DZero at Fermilab (See Section 3.2). Besides not observing the Higgs boson, these experiments placed very useful constraints on some of the Higgs boson parameters such as the mass. For example, LEP experiments showed with a confidence level of 95% that the Higgs boson could only be observed at masses greater than 114.4 GeV. Fermilab experiments also performed a 95% confidence level exclusion of Higgs masses in the range 162 to 166 GeV. Such constraints led to the creation of suitable experiments at the LHC which then led to the recent discovery of the Higgs-like boson.

[3] Spontaneous symmetry breaking of a continuous global symmetry is always accompanied by the appearance of one or more massless scalar particles called Goldstone bosons. In the example used here, the goldstone boson is associated with the field M.

2. The LHC and the ATLAS Detector

The need for extremely high energies as a prerequisite to the discovery of the Higgs boson led to the development of the world's largest particle collider: the Large Hadron Collider (LHC).

The LHC ring is about 27 km in circumference and is located at about 100 m underground at the Franco-Swiss border. This amazingly large particle collider, administered by the European Organization for Nuclear Research (CERN), was designed to collide protons at energies of up to 14 TeV. It has two opposing particle beams that intersect at four interaction points, each having a detector to detect the outcome of the interactions. These detectors are namely: A Toroidal LHC Apparatus (ATLAS) [Col08b], Compact Muon Solenoid (CMS) [Col08d], A Large Ion Collider Experiment (ALICE) [Col08a] and LHC Beauty (LHCb) [Col08e]. The ATLAS and CMS detectors are general purpose detectors where as ALICE and LHCb are dedicated detectors. The ALICE detector is dedicated to the studies of Quark Gluon Plasma (QGP), a state of matter in which quarks and gluons appear to be in a deconfined state. Lead nuclei collisions are especially essential in this study. The LHCb detector is dedicated to the study of b-quark physics. In addition to these main detectors, the LHC has three other detectors that are much smaller and carry out specialized research. These these include the Total Cross Section, Elastic Scattering and Diffraction Dissociation (TOTEM) [Col08g], LHC forward (LHCf) [Col08f] and Monopole and Exotics Detector At the LHC (MoEDAL).

This chapter highlights the main features and functions of the LHC and the ATLAS detector, that make them key tools in making such excellent discoveries as the discovery of the Standard Model Higgs-like boson. Sections 2.1 and 2.2 describe the LHC and the ATLAS detector respectively. Most of the information used is based on [EB08] for the LHC and [Col08b] for the ATLAS detector.

2.1 The Large Hadron Collider

The LHC is both a proton-proton (p-p) collider and a lead nuclei (Pb-Pb) collider. It's engineering began in 1998, with a vision to create an extremely high energy machine to answer some of the pending questions in physics such as the existence of the Standard Model Higgs boson and supersymmety, as well as to discover totally new physics. By September 2008, it was commissioned and successfully collided the first p-p beams before it went on a temporary shut down due to a magnet quench and subsequent loss of helium which destroyed several superconducting magnets

which aid the bending of particle beams as explained below. When it resumed operations in 2009, it operated at a center of mass energy of about 2 TeV. With the ongoing upgrades being conducted in 2013 and 2014, the LHC is expected to run at its design energy of 14 TeV in 2015. Fig. 2.1 shows a schematic diagram of the LHC showing the main detectors. In order to achieve

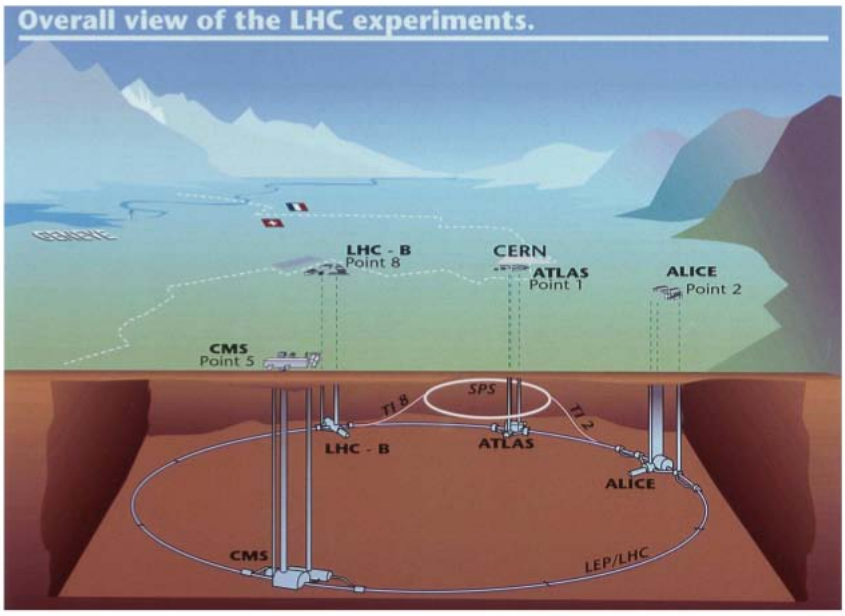

Figure 2.1: The Large Hadron Collider [Mos11]

the enormous amounts of energy needed, the particle beams are passed through a series of particle accelerators that prepare them for injection into the LHC. Firstly, the proton or lead nuclei beams are released from a source into the Linear Accelerator (LINAC) which then accelerates them into a Booster once they have reached about 500 MeV. The Booster further accelerates them to about 1.4 GeV before injecting them into the Proton Synchrotron (PS). From the PS, the beams are injected into the Super Proton Synchrotron where they are accelerated to about 450 GeV before they are finally injected into the LHC. In the LHC, the beams are accelearated to about 4 TeV per beam (i.e for a center of mass energy of 8 TeV, for example). This takes approximately 25 minutes and they are designed to circulate around the beam pipe while colliding at the interaction points. Once a substantial part of the beam has been lost to collisions, the beams are dumped and replaced with new ones. This procedure takes place about once daily. On average, heavy-ion collisions are only included for about one month per year. To keep the beams moving in a circular path, over 1232 superconducting dipole magnets with a magnetic field of 8.4 Tesla are used. In addition, about 390 quadrupole magnets are used to keep the beams focussed. These magnets are cooled by liquid helium to about 1.9 K.

The design luminosity of the LHC is 10^{34} cm^{-2} s^{-1}, providing a rate of about 40 million p-

p collisions per second. The instantaneous luminosity is defined as the number of collisions produced per unit area per unit time in a particle detector and hence determines the intensity of a beam and integrated luminosity is referred to as the number of interactions, N, occuring in a given total cross section area, σ. Integrated luminosity determines the productivity of a collider and its relationship to the number of interactions produced per total cross section area is given by Equation 2.1.1.

$$\int Ldt = \frac{N}{\sigma} \tag{2.1.1}$$

2.2 The ATLAS Detector

The ATLAS detector is the world's largest particle detector for collision experiments, with a length of 45 m, a height and width of 25 m and a weight of about 7000 tons. It is a general purpose detector with a wide range of objectives. Like most particle detectors, ATLAS is structured in an onion-like fashion. It has multiple layers or detector components each of which has a specific role in the detection process. It's main components are the inner detector trackers, the calorimeters, the muon chambers and the magnetic systems. Fig. 2.2 shows the structure of the ATLAS detector.

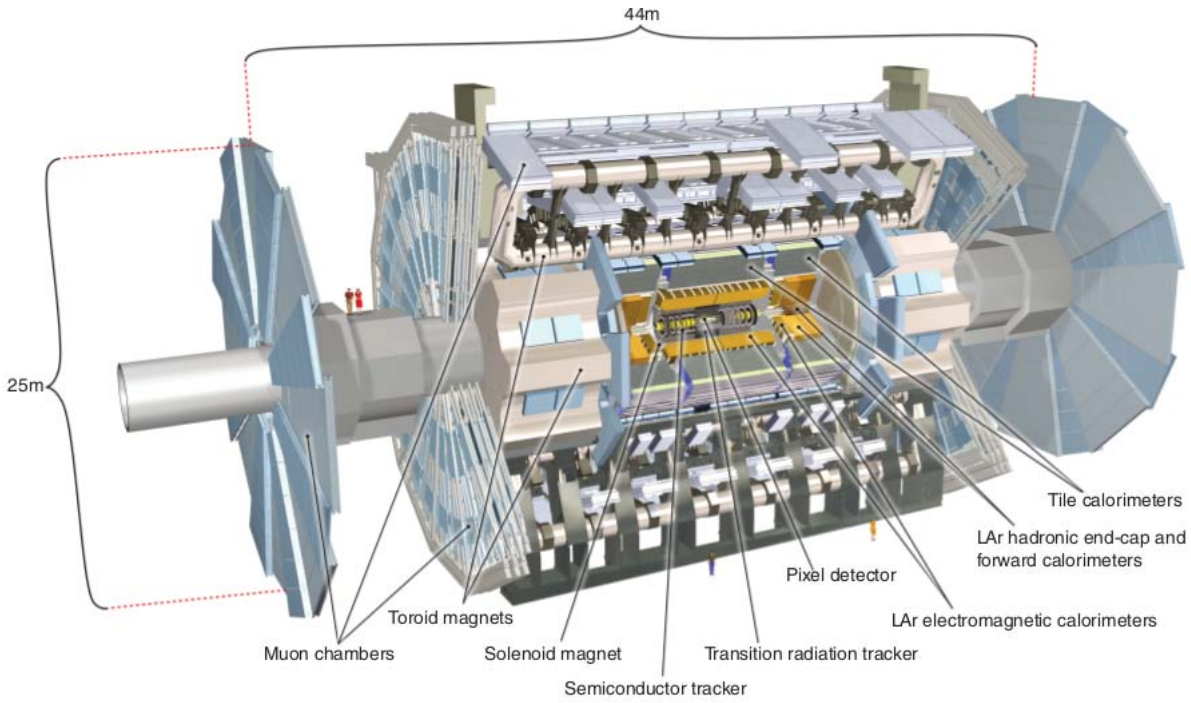

Figure 2.2: The ATLAS detector [Col08b].

The inner detector's main function is to identify and measure the momentum of charged particles. It is a very high precision component with a radius of 1.2 m and a length of 6.2 m along the beam pipe. It's composed of three main parts: the pixel detector, the semiconductor tracker (SCT) and the Transition Radiation Tracker (TRT). The innermost component, the pixel detector, contains silicon which acts as its detection material and has a number of readout chips to read the particle information. The SCT is also a silicon detector but with a larger radius and larger silicon area than the pixel detector. On the other hand, TRT uses drift tubes as its detection element. In addition, the entire inner detector is surrounded by a magnetic field which bends the trajectory of charged particles and helps determine the charge and momentum of the particle. The inner detector magnets are then followed by the calorimeter system, composed of two types of calorimeters. These are the electromagnetic and hadronic calorimeters, which both measure the energies deposited by particles as they interact with the calorimeter material. The electromagnetic calorimeter measures the energy deposited by particles that interact via the electromagnetic interaction whereas the hadronic calorimeters measure the energy deposited by particles that interact via the strong interactions. The calorimeters are made up of a number of cells such that when a particle interacts with the calorimeter's material, it deposits energy in many different calorimeter cells. Outside the calorimeter system is the muon spectrometer which is designed to identify muons and measure their momentum. The muon spectrometer is surrounded by a magnetic field provided by toroidal magnets.

2.2.1 The ATLAS Coordinate System. Fig. 2.3 shows a shematic diagram of the ATLAS coordiante system. The origin is taken to be at the center of the detector (the interaction point). The z-axis is taken to be along the beam pipe and the x and y axes are towards the center of the LHC and upwards, respectively. In Fig. 2.3, ϕ is the azimuthal angle around the beam pipe and θ is the angle between the track of a particular particle and the z-axis. This angle can also be represented in a different form as illustrated in Equation 2.2.1. This is known as the pseudorapidity. The distance in the $\eta - \phi$ plane, $\triangle$R, is defined according to Equation 2.2.2.

$$\eta = -\ln\left[\tan\left(\frac{\theta}{2}\right)\right] \tag{2.2.1}$$

$$\triangle \mathrm{R} = \sqrt{\triangle\phi^2 + \triangle\eta^2} \tag{2.2.2}$$

Defining the coordinate system in this way helps to determine the exact position coordinates of particles at a particular point in space and aids in the reconstruction and identification of particles. The radii, lengths and pseudorapidity coverages of the various detector components of the ATLAS detector are shown in Table 2.1. Subsection 2.3 briefly describes the various signatures left by some particles as they traverse through the detector and how they are identified.

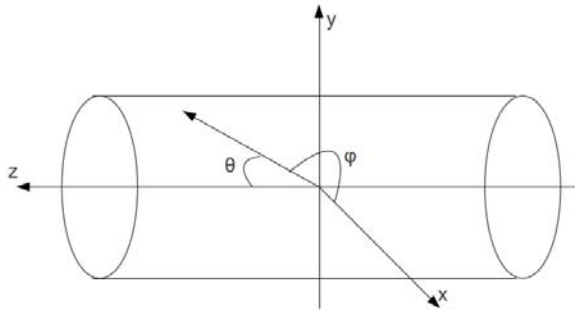

Figure 2.3: ATLAS Coordinate System.

Component	Radius $[m]$	Length $[m]$	$\eta-$coverage
Barrel muon spectrometer	11	26	$\|\eta\| < 1.4$
End-cap muon spectrometer	11	2.8	$1.1 < \|\eta\| < 2.8$
Barrel hadronic calorimeter	4.25	12.2	$\|\eta\| < 1.0$
End-cap hadronic calorimeter	2.25	2.25	$1.5 < \|\eta\| < 3.2$
Barrel em-calorimeter	2.25	6.42	$\|\eta\| < 1.4$
End-cap em-calorimeter	2.25	0.63	$1.4 < \|\eta\| < 3.2$
Forward/Backward calorimeter	integrated in end-cap		$3.1 < \|\eta\| < 4.9$
Barrel + end-cap inner detector	1.15	6.8	$\|\eta\| < 2.4$

Table 2.1: Pseudorapidity coverage of the ATLAS sub-detectors [Dan98].

2.3 Particle Reconstruction and Identification

Particles emerging from a p-p collision leave characteristic signatures in the detector, depending on their interactions with the various detector components mentioned above. This makes their identification possible. For example, a proton interacts in the hadronic calorimeter, where it deposits a cluster of energy and leaves a track along its path from the inner detector. Similarly, a neutron interacts in the hadronic calorimeter but it leaves no track along its path from the inner detector. However, since protons and neutrons are composite particles of quarks which can only occur in bound states, protons and neutrons are identified from hadronic jets in the hadronic calorimeter. These jets are formed by the hadronization of quarks and gluons. Electrons and photons interact in the electromagnetic calorimeter, with the electron leaving a track in the inner detector and the photon leaving no track. A neutrino goes through the entire detector without leaving a track and thus can only be identified from the imbalance of the tranverse energy and momentum in an event. Unlike neutrinos, muons traverse the entire detector while leaving tracks behind. Detector components known as muon chambers located in the end-cap region are specifically designed to determine the kinematics of muons using muon tracks. Fig. 2.4 shows a

pictorial summary of the signatures left by various particles as they travel through the detector.

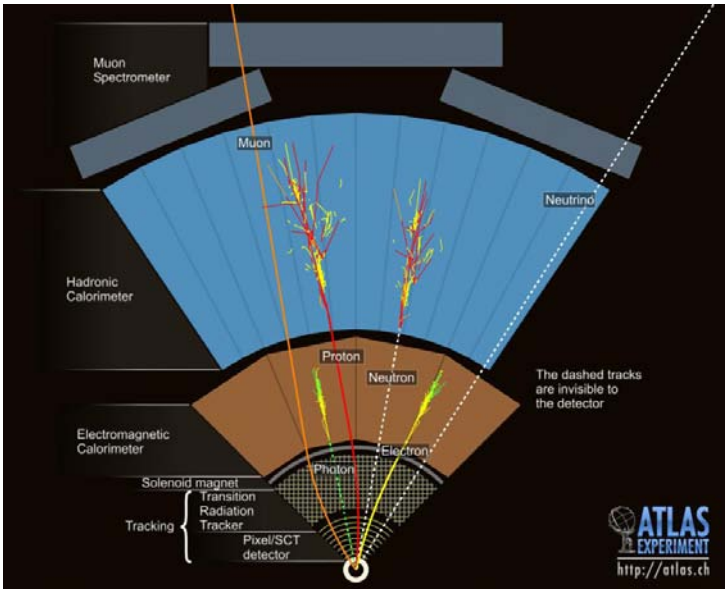

Figure 2.4: Particle Identification [Vir12].

The detector records the information from particle interactions, as electronic signals. Therefore, prior to a particle's identification, this information has to be reconstructed in order to interpret the signals into original particles, their momenta, directions and the event's primary vertex. The primary vertex is referred to as the point at which a particle from one particle beam interacts with another particle from the opposite particle beam. When particles emerging from the primary vertex decay, these decay points are referred to as secondary vertices. In most cases, more than one primary vertex is recorded at the same time. These multiple interactions are referred to as pile up interactions.

To illustrate reconstruction and identification of particles, the following sections describe the reconstruction and identification of electrons and photons (2.3.1) as well as jets (2.3.2) and missing transverse energy (2.3.3).

2.3.1 Reconstruction and Identification of Electrons and Photons. The material used in this section is referenced from [Col08c], [ftAc08] and [Ali12]. According to these references, the reconstruction of electrons and photons is done using information from both the electromagnetic calorimeter and the inner detector. The commonly used reconstruction algorithm for electrons and photons is the 'egamma' reconstruction algorithm. In ATLAS, the signature of an electron is a reconstructed track in the inner detector, associated to a narrow, localized cluster of energy in the electromagnetic calorimeter. Photons are only reconstructed in the electromagnetic calorimeter since they do not leave tracks in the inner detector. The energy deposited in the various cells

of the calorimeter are grouped into energy clusters using clustering algorithms. These clusters are then reconstructed using an algorithm that scans a fixed size rectangular window over the $\eta - \phi$ grid of calorimeter cells, searching for a local maxima of energy contained in the window. To begin with, seed clusters with a window size of 5×0.025 units in the $\phi-$space and 3×0.025 in the $\eta-$space are reconstructed. These seed clusters are required to have a transverse energy of at least 2.5 GeV. To distinguish an electron from an unconverted photon, the clusters are matched to tracks reconstructed in the inner detector. In order to form an electron candidate, atleast one track is required to fall within $\triangle\eta$ <0.05 and $\triangle\phi$ <0.1 of the reconstructed seed cluster. In case of multiple tracks matching the cluster, the track with the closest $\triangle$R is chosen. To distinguish an electron from a converted photon, the inner detector tracks are matched to a secondary vertex. After track matching, the seed clusters of the electron candidates are rebuilt and the electron energy is determined. At this stage, electron candidates are reffered to as reconstructed electrons. In order to use electrons and photons effectively, and to distinguish each of them from jet processes that fake signatures of electrons or photons, various identification criteria are applied to the reconstructed electrons. A standard identification procedure involves applying particular cuts to discriminating variables known as shower shape variables. The cuts are categorised into loose, medium and tight identification cuts, with the loose cuts having minimal identification requirements. These cuts are further optimized, depending on the type of analysis being done.

Fig 2.5 shows pictures of a reconstructed electron (a) and a reconstructed photon (b) in the ATLAS detector.

2.3.2 Reconstruction and Identification of jets. For most particle physics analyses, excellent reconstruction of jets and missing transverse energy is required. Several reconstruction algorithms are used in the reconstruction of jets and missing transverse energy. Jets result from QCD interactions and they define the hadronic final states of any physics channel. On the other hand, events with large E_T^{miss}, in the ATLAS detector, are expected to provide information on exotic physics like dark matter as well as new physics such as supersymmetry and extra dimensions. This section describes some details of the reconstruction algorithms used by ATLAS to reconstruct jets. Reconstruction algorithms for missing transverse energy are described in section 2.3.3. In each case, the calorimeter system plays a principal role. The description of these algorithms is obtained from reference [Col08c].

The most commonly used jet finder algorithms in ATLAS are the seeded fixed cone finder and the sequential recombination algorithms. The theoretical and experimental requirements of the algorithm are also listed in [Col08c]. This analysis uses jets reconstructed by sequential recombination algorithms. In the implementation of the seeded fixed cone finder, the basic idea is to

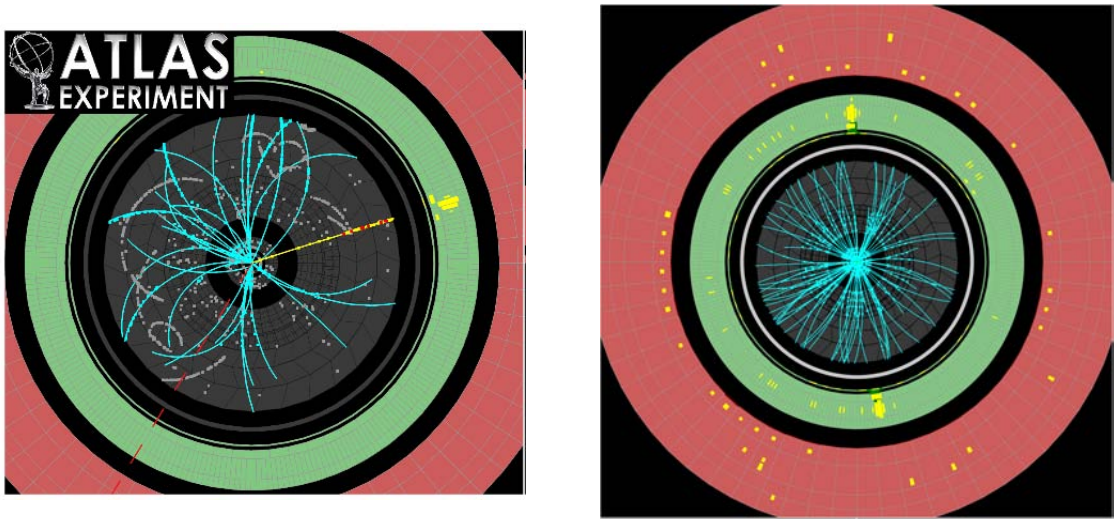

(a) Reconstructed electron

(b) Reconstructed photon

Figure 2.5: (a) Event display of a reconstructed electron from a candidate W decay. The electron cluster is shown in yellow, in the green electromagnetic calorimeter [Ali12]. (b) Event display of a reconstructed diphoton pair. The photon clusters are shown in yellow in the green electromagnetic calorimeter [Col12b]. In both pictures, the blue lines represent inner detector tracks and the red dotted lines in (a) represent E_T^{miss}.

find stable cones in the $\eta - \phi$ plane. All input objects from an event are ordered in decreasing p_{T}. All objects within a cone in η and ϕ with $\triangle$R$<$ R$_{cone}$, where R$_{cone}$ is the fixed cone radius (0.4$\leq$R$_{cone}$ $\leq$0.7), are combined with the cluster seed in the calorimeters, provided that the object with the highest p$_T$ is above the seed threshold. A seed threshold of p$_T$ $>$1 GeV is used. A new direction is calculated from the 4-momenta inside the initial cone and a new cone is centered around it. Objects are then re-collected in this new cone, and again the direction is updated. This process continues until the direction of the cone does not change anymore after recombination, at which point the cone is considered stable and is called a jet. At this point the next seed is taken from the object input list and a new cone jet is formed with the same iterative procedure. This continues until no more seeds are available. This algorithm is easy to implement and is fast, hence its the most commonly used. However, it is only meaningful to leading order for inclusive jet cross-section measurements and final states like W or Z+1 jet, and not at any order for 3-jet final states, W or Z+2 jets, and for the measurement of the dijet invariant mass in 2-jets+X final states. In addition, because it is seeded, this algorithm is not infrared safe (See the theoretical requirements in [Col08c]).

For the implementation of the sequential recombination algorithm in ATLAS, the anti-k_T algorithm is used [MG08]. In this algorithm, all pairs, ij, of input event objects such as partons,

particles, reconstructed detector objects with four-momentum representation, are analyzed with respect to their relative transverse momentum squared defined in Equation 2.3.1. In addition, the squared p_T of object i relative to the beam, $d_i = p^2_{T,i}$ is used. With these definitions, the minimum, d_min of all $d_{i,j}$ and d_i is found, such that if d_{min} is a d_{ij} , the corresponding objects i and j are combined into a new object, k, using 4-momentum recombination. Thereafter, the objects i and j are removed from the list, and the new object k is added to it. On the other hand, if d_{min} is a d_i, the object i is considered to be a jet by itself and is removed from the list. This procedure is repeated for the resulting new sets of d_{ij} and d_i until all objects are removed from the list. This means that all original input objects end up to be either part of a jet or to be jets by themselves. it does not use seeds, it is also collinear safe. The distance parameter R, which is the only free parameter besides the choice of recombination scheme in this inclusive implementation of the anti-k_T algorithm, allows some control on the size of the jets. Default configurations in ATLAS are R = 0.4 for narrow and R = 0.6 for wide jets. This algorithm is slow. However, it has an advantage of being infrared safe.

$$d_{i,j} = min(p^2_{T,i}, p^2_{T,j}) \frac{\triangle\eta^2_{i,j} + \triangle\phi^2_{i,j}}{R^2} \tag{2.3.1}$$

Figure 2.6 (a) shows a reconstructed jet in ATLAS.

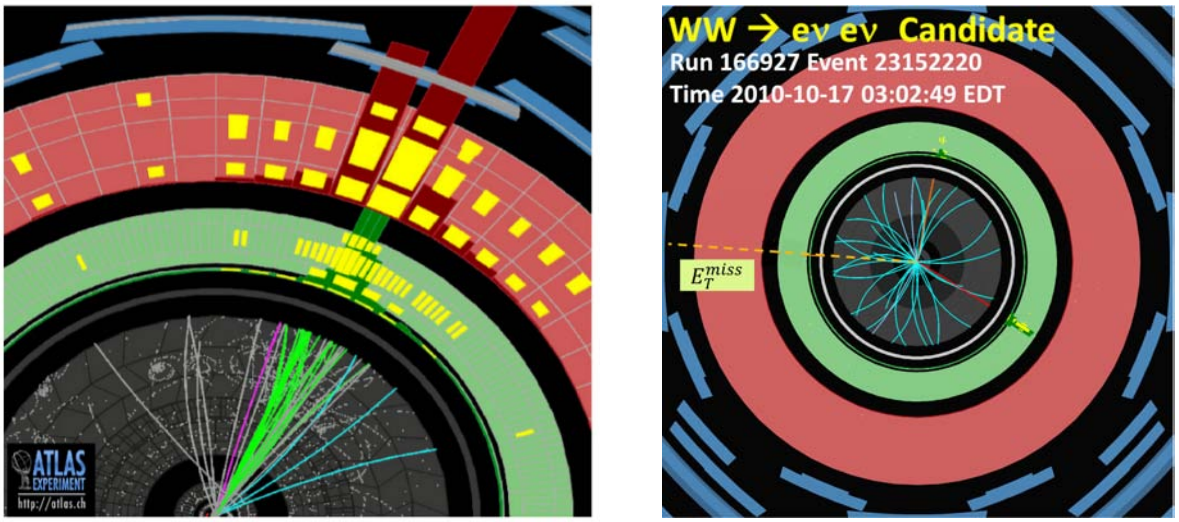

(a) Reconstructed jet

(b) Reconstructed missing transverse energy

Figure 2.6: (a) Event display of a reconstructed jet in the transverse plane [col13b] of the ATLAS detector. (b) Event display of reconstructed missing transverse energy in the ATLAS detector [Col11a].

2.3.3 Reconstruction and Identification of Missing Transverse Energy. In the case of E_T^{miss}, reconstruction is done using energy deposits in the calorimeter and reconstructed muon

tracks (The reconstruction of muons is also decsribed in [Col08c]). To illustrate this, a simple refined reconstruction procedure obtained from [ftAc12] is described. This procedure is illustrated in detail in [Col08c] and is categorized into two categories: cell-based and object-based reconstructions. To begin with, the sum of the two E_T^{miss} components from the calorimeter and muon tracks is given by Equation 2.3.2. The calorimeter term is reconstructed using calorimeter cells calibrated according to the reconstructed physics object to which they belong. Calorimeter cells are associated with a reconstructed and identified high p_T parent object in a chosen order: electrons, photons, hadronically decaying τ-leptons, jets and muons. Cells not associated with any such objects are also taken into account in the calculation of E_T^{miss}. Once the cells are associated with these objects, the calorimeter term is calculated according to Equation 2.3.3. In this equation, each term is calculated from the negative sum of calibrated cell energies inside the corresponding objects as shown in Equation 2.3.4, where E_i, θ_i and ϕ_i represent the energy, the polar angle and the azimuthal angle. The first three terms in Equation 2.3.3 are respectively reconstructed from cells in clusters associated to electrons, photons and τ-jets from hadronically decaying τ-leptons. The fourth term is reconstructed from cells in clusters associated to calibrated jets with $\mathrm{p}_T > 20$ GeV. The fifth term is reconstructed from cells in clusters associated to jets with 7 GeV $< \mathrm{p}_T < 20$ GeV. Finally, the last two terms are the contribution to E_T^{miss} originating from the energy lost by muons in the calorimeter and E_T^{miss} from cells in topoclusters which are not included in the reconstructed objects, respectively.

$$\mathrm{E}_{x,y}^{miss} = \mathrm{E}_{x,y}^{miss,calo} + \mathrm{E}_{x,y}^{miss,\mu} \tag{2.3.2}$$

$$\mathrm{E}_{x,y}^{miss,calo} = \mathrm{E}_{x,y}^{miss,e} + \mathrm{E}_{x,y}^{miss,\gamma} + \mathrm{E}_{x,y}^{miss,\tau} + \mathrm{E}_{x,y}^{miss,jets} + \mathrm{E}_{x,y}^{miss,softjets} + \mathrm{E}_{x,y}^{miss,calo,\mu} + \mathrm{E}_{x,y}^{miss,CellOut} \tag{2.3.3}$$

$$\mathrm{E}_x^{miss,term} = -\sum_{i=1}^{N_{cell}^{term}} \mathrm{i} \sin\theta_i \cos\phi_i \quad \text{and} \quad \mathrm{E}_y^{miss,term} = -\sum_{i=1}^{N_{cell}^{term}} \mathrm{i} \sin\theta_i \sin\phi_i \tag{2.3.4}$$

See Figure 2.6 (b) for the reconstructed missing transverse energy in ATLAS. Similar to the electrons and photons, events with jets and missing transverse energy are further identified and optimized by event selection criteria depending on the type of physics analysis.

2.3.4 The Trigger System. As mentioned in section 2.1, at it's design luminosity, the LHC would operate at a maximum of about 40 million bunch crossings per second $(40\mathrm{MHz})$, with collisions occuring every $25\mathrm{ns}$. This would lead to a very large amount of data, all of which can not be stored. Infact, despite the LHC not reaching its full luminosity yet, it has been able to produce significantly large amounts of data. However, due to limited storage, not all events can be stored. Therefore, only events reflecting interesting properties for a particular physical process

are selected. This is done by a computer system known as the trigger system which is made up of three levels [vE07].

The first trigger level (LVL1) is hardware-based and is designed to reduce the nominal data-taking rate to about 75 kHz. Events accepted by the LVL1 trigger are then passed to the second level trigger (LVL2). LVL2 is software-based and uses the full event information to further reduce the data to about 1 kHz. Finally, the third level trigger (LVL3) imports data from LVL2 and uses reconstruction algorithms to fully reconstruct the events and hence reduce the data volume to only about 600 Hz. This corresponds to about 600 MB/s of data, which is then stored for further offline reconstruction before sending it to storage facilities and made available for physics analysis.

3. The Search For The Higgs Boson

Statistical analysis techniques have been a cornerstone of experimental particle physics for several decades. The general statistical tools used in particle physics to discover new particles and to set limits on parameters such as mass, are presented in section 3.1 of this chapter. Some searches for the Higgs boson conducted at earlier experiments prior to the creation of the LHC are presented in section 3.2. Searches conducted at the LHC's ATLAS detector prior to the discovery of the Higgs-like particle and those that led to the discovery are also presented in section 3.3. Finally, the search for an invisibly decaying Higgs boson at ATLAS is presented in section 3.4.

3.1 Statistical Methods For Particle Physics Analysis

The quantitative comparison of theories with observations is an important part of particle physics because it leads to validating or refuting the theories. Statistical techniques play a major role in doing this by testing hypotheses and fitting their underlying parameters. In the past years, statistics has highly contributed in analyses involving the Standard Model Higgs boson. It helped set limits on the unknown mass parameter of the Higgs boson and finally led to its discovery. Statistics still remains a major contributing factor to the analysis of the many properties of the Higgs boson currently being explored.

For statistical tests, either Bayesian methods or frequentist methods are employed. The former defines probability based on a degree of belief. Prior knowledge of the observed data and the parameters affecting it is required and the solution to an inference problem is provided by the posterior probability distribution of the parameter of interest. This approach is, however, beyond the scope of this thesis. Details on Bayesian methods in particle physics can be obtained from references [Cas11], [Cra]. On the otherhand, frequentist methods define probability based on the repeatability of an experiment. Since particle physics experiments involve several repeated collisions of particles, their analyses have so far widely used frequentist methods. In the frequentist approach, one seeks to accept or reject a given hypothesis. The merits and demerits of each approach is widely discussed in the community.

This section highlights some of the general frequentist statistical procedures followed in particle physics analyses. Most of the material used here is obtained from [eta10], [Cra], [Cas11], [L.R00].

3.1.1 Building a Statistical Model. Statistical tests are preceded by building a statistical model of the data. A statistical model is a mathematical representation of the data and all the factors affecting it. Developing it involves an understanding of the physics of the data and the details of the experiment.

Most particle physics experiments are based on counting events of particular interest. However, besides counting events, some experiments also involve additional measured quantities such as the invariant mass of a particle. The data is often represented in histograms, leading to binned analysis techniques. In what follows, the binned technique is illustrated.

As an example, if the Higgs mass, m_H, is being studied, a histogram, $n = (n_1, \ldots, n_N)$ of the mass is constructed, where n_1 represents the number of events in the the first bin, i.e at mass m_{H_1}. The expectation value of the number of events in bin i of the histogram, $E[n_i]$, is given by Equation 3.1.1, where μ determines the strength of the signal process. $\mu = 0$ corresponds to the background-only hypothesis and $\mu = 1$ is the nominal signal hypothesis. s_i and b_i are the mean number of entries in bin i from signal and background respectively.

$$E[n_i] = \mu s_i + b_i \tag{3.1.1}$$

In this case, all statistical tests are based on μ, since it acts as a scaling factor on the total number of events predicted by the Standard Model for a particle's signal. In other words, μ is the parameter of interest and all other parameters such as shape uncertainties, detector systematics and theoretical uncertainties are considered nuisance parameters, θ. In order to constrain the nuisance parameters, an additional histogram, $k = (k_1, \ldots, k_K)$, is obtained from control regions which are expected to consist of only background. In this case, the expectation value of the number of events in bin j of this histogram, $E[k_j]$, is given by Equation 3.1.2 where u_j are functions of θ that can be calculated. Once a particular set of data has been obtained, the probability, as a function of μ and θ, of observing that data is given by the likelihood function, $L(\mu,\theta\,)$. The likelihood function can be expressed by the product of Poisson probabilities for all bins as shown in Equation 3.1.3. Likelihood-based frequentist statistical tests are commonly used in particle physics analyses.

$$E[m_j] = u_j(\theta) \tag{3.1.2}$$

$$L(\mu,\theta\,) = \prod_{i=1}^{N} \frac{(\mu s_i + b_i)^{n_i}}{n_i!} \exp\left(-(\mu s_i + b_i)\right) \prod_{j=1}^{K} \frac{u_j^{k_j}}{k_j!} \exp\left(-u_j\right) \tag{3.1.3}$$

The probability distribution of a particular value of m_H, given μ and θ is known as the probability density function (pdf) of m_H or probability model of m_H and is written as $f(m_H|\mu,\theta\,)$. Such a

distribution is obtained by running pseudo experiments or by using an artificial dataset called the Asimov dataset [eta10]. Now, considering that events occur independently, the overall pdf for a particular dataset ($D = m_{H_1}, m_{H_2}, ..., m_{H_N}$) is the product of the pdfs of each individual event in the dataset. In addition, if the number of expected events from various signals and backgrounds is known, then the overall probability model of m_H is multiplied by the Poisson probability for observing n events given ν expected. The resulting model is called a marked Poisson model and is expressed in Equation 3.1.4. This model contains all the information about the observed data, the expected data and the parameters.

$$f(D|\nu,\mu,\theta) = Poisson(n|\nu,\mu,\theta) \prod_{i}^{n} f(m_{H_i}|\mu,\theta) \tag{3.1.4}$$

Once the model has been built, the statistical tests on the observed data proceed by extracting particular information from the model. In the likelihood-based approach, the test statistic used on a hypothesized value of μ is the profile likelihood ratio, $\lambda(\mu)$. A test statistic is a function that quantifies the difference between the data and the null hypothesis and profiling refers to the procedure of setting specific values of nuisance parameters for a given μ and data. Equation 3.1.5 shows the profile likelihood ratio. This is the ratio of the conditional maximum likelihood to the unconditional maximum likelihood. In the conditional maximum likelihood, $\hat{\hat{\theta}}$ denotes the value of θ that maximizes the likelihood for the specified μ. Whereas $\hat{\mu}$ and $\hat{\theta}$, in the unconditional maximum likelihood, are the unconditional maximum likelihood estimators. The test statistic, q_μ, expressed in Equation 3.1.6 is also used, such that $q_\mu = 0$ implies good agreement between the hypothesized value of μ and the observed data.

$$\lambda(\mu) = \frac{L(\mu, \hat{\hat{\theta}})}{L(\hat{\mu}, \hat{\theta})} \tag{3.1.5}$$

$$q_\mu = -2ln\lambda(\mu) \tag{3.1.6}$$

To quantify the level of agreement between the observed data and the hypothesis, the p-value can be used [Cra]. The p-value gives the probability, under the assumption of the null hypothesis, of observing a result at least as extreme as the test statistic. Equation 3.1.7 shows the expression for the p-value, where $q_{\mu,obs}$ is obtained from the data and $f(q_\mu|\mu)$ is the probability density function of q_μ.

$$p_\mu = \int_{q_{\mu,obs}} f(q_\mu|\mu) dq_\mu \tag{3.1.7}$$

3.1.2 Establishing Discovery. Inferring the presence of a signal is achieved from the difference between the observed event rate and that expected from background processes alone.

Background-only implies that $\mu = 0$, such that the hypothesized value of μ is zero. The p-values are calculated at each m_H value in a given range. They are then interpreted in terms of the significance, Z, as expressed in Equation 3.1.8, where ϕ^{-1} is the quantile of the normal distribution. The quantile function is the inverse of the cumulative distribution function. In particle physics, a p-value of less than 2.7×10^{-7}, corresponding to $\mathrm{Z} \geq 5\sigma$, is considered sufficient to declare a discovery. Here, σ represents the standard deviation. A significance lying in the range $3\sigma \leqslant \mathrm{Z} < 5\sigma$ indicates evidence for a discovery and that lying in the range $\mathrm{Z} < 3\sigma$ is referred to as a statistical fluctuation.

$$\mathrm{Z} = \phi^{-1}(1 - \mathrm{p}_0) \tag{3.1.8}$$

3.1.3 Setting Limits. Besides establishing discovery by rejecting the $\mu = 0$ hypothesis, limits can also be imposed on other non-zero μ values, especially when the background processes are very large. In this case, the signal + background hypothesis becomes the null hypothesis and the background-only hypothesis is taken as the alternative hypothesis. The p-value is computed for each μ value and the set of μ values whose p-values exceed 1-CL for a particular confidence level (CL), sets a confidence interval for μ. A confidence level gives an estimated range of values which is likely to include an unknown population parameter. If a confidence level of 95% is being considered, then μ values whose p-values exceed 0.05 are excluded at 95%CL. Since one seeks to determine the smallest μ value that is compatible with the data at 95%CL, the test statistic used for limit setting is given by Equation 3.1.9. The data with $\hat{\mu} > \mu$ are not considered as they would correspond to other larger values of μ.

$$q_\mu = \begin{cases} -2ln\lambda(\mu) & \hat{\mu} \leq \mu \\ 0 & \text{otherwise} \end{cases} \tag{3.1.9}$$

To set limits on the mass of a particle, for example m_H for Higgs mass, the m_H value corresponding to an excluded μ value is also excluded. Fig 3.1 gives an example of limits set in the combined search for the Standard Model Higgs boson in the ZZ, WW and diphoton decay channels. In this plot, each m_H value corresponding to a 95%CL on μ that is below the expected from backgroud, is excluded. On the other hand, an observed 95%CL on μ that exceeds the $+2\sigma$ band of the expected background, indicates an excess of events at its corresponding mass. In this figure, an excess of events is observed at around 125 GeV hence the observation of a Higgs-like particle at 125 GeV.

Another commonly used technique for limit setting in particle physics is the $\mathrm{CL_s}$ technique. It gives an approximation to the confidence in the signal hypothesis, that one might have obtained if the experiment was performed in the complete absence of background. It is based on the test

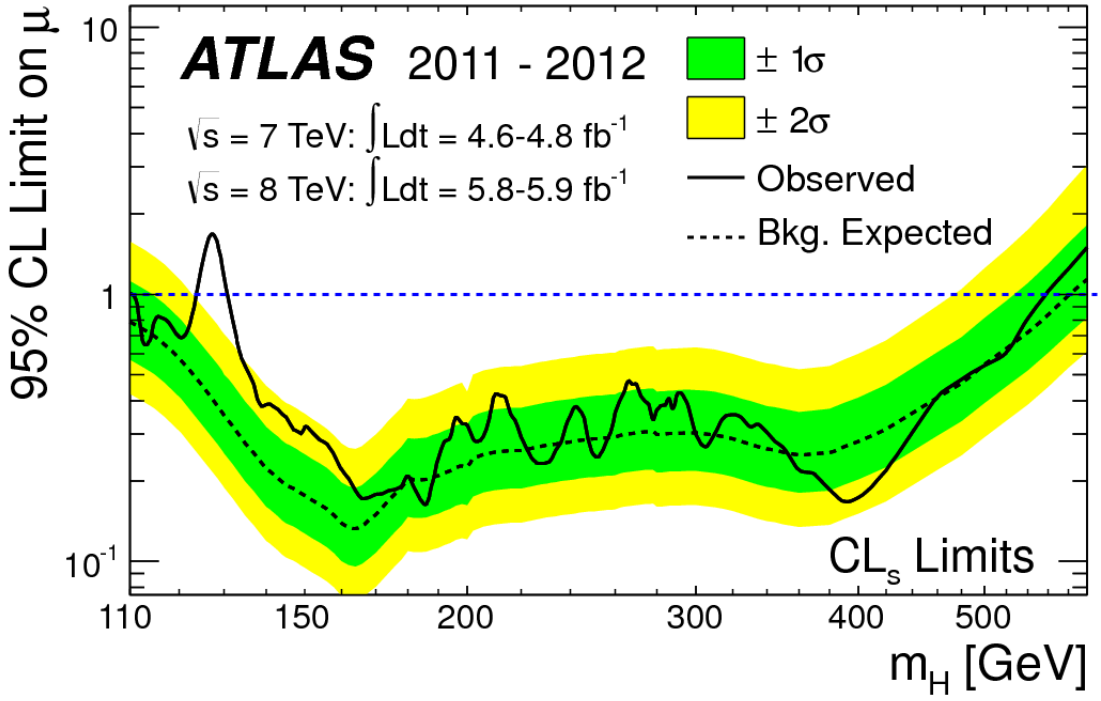

Figure 3.1: Example: The observed and expected 95% confidence level limits on μ for the combined search of the Higgs boson for the period 2011-2012 [Col12a].

statistic q_μ defined by Equation 3.1.10, where p_{s+b} represents the probability, under the signal + background hypothesis, of obtaining a test statistic of equal or greater value to the one observed from experiment and p_b represents the probability, under the background-only hypothesis, of obtaining a test statistic of equal or lesser value to the one observed from experiment. The mathematical representations of p_{s+b} and p_b are given in Equations 3.1.11 and 3.1.12. A signal model is regarded as excluded, at 95%CL, if $\mathrm{CL_s} \leq 0.05$.

$$\mathrm{CL_s} = \frac{p_{s+b}}{1 - p_b} \tag{3.1.10}$$

$$p_{s+b} = P(q_\mu \geq q_{\mu,obs}|s+b) = \int_{q_{\mu,obs}}^{\infty} f(q_\mu|s+b)dq \tag{3.1.11}$$

$$p_b = P(q_\mu \leq q_{\mu,obs}|b) = \int_{-\infty}^{q_{\mu,obs}} f(q_\mu|b)dq \tag{3.1.12}$$

Details on the implementation of statistical techniques for setting limits are illustrated in Chapter 4 as this was a major component of this study.

Some earlier results obtained prior to the discovery of a Higgs-like particle from various experiments which set constraints on the mass of the SM Higgs are highlighted in section 3.2 below.

Section 3.3 presents the production and decay modes of the Higgs at the LHC and shows results of the discovery of the Higgs-like particle at ATLAS. Section 3.4 shows recent results obtained from searches of an invisibly decaying Higgs at ATLAS.

3.2 Results From Earlier Experiments

The Large Electron-Positron collider at CERN (LEP), a predecessor to the LHC, was one of the experiments that published concrete results on the limits set on the Higgs mass. It operated from the year 1989 to the year 2000 when it paved way for the creation of the LHC. LEP consisted of four collision points each of which housed a single experiment namely ALEPH, DELPHI, L3 and OPAL [MM02]. By the time LEP was shut down, large amount of data corresponding to center of mass energies of up to 209 GeV had been collected. With this data, a combined search for the Higgs boson from LEP's four collaborations excluded Higgs masses less than 114.4 GeV at a confidence level of 95%. This result is shown in Fig. 3.2. In this figure, CLs represents the probability to obtain a configuration of events which is more signal-like given the observed data. The lowest test mass giving CLs = 0.05 is taken to be the lower bound on the mass at 95% confidence level.

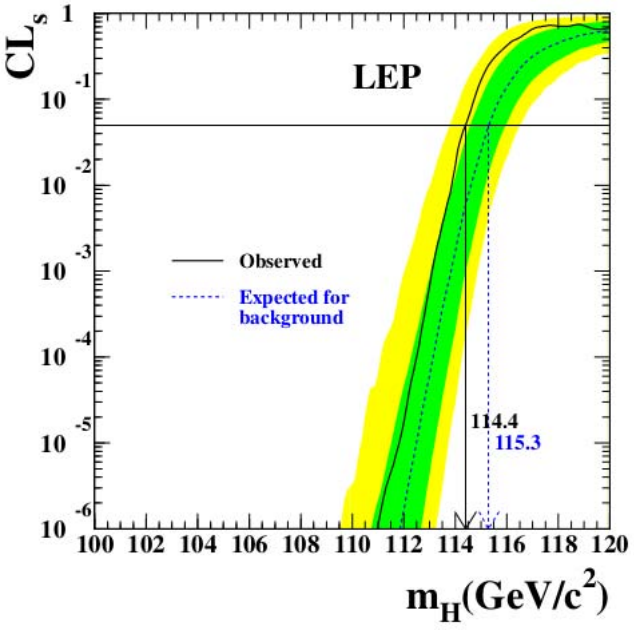

Figure 3.2: A lower limit of $114.4\mathrm{GeV}$ set on the Higgs mass by LEP experiments [Sea03].

The Tevatron at the Fermi National Laboratory (Fermilab) was also on the hunt for the Higgs boson. The Tevatron was a circular proton-antiproton accelerator with two main collaborations;

CDF and DO (DZero). It was shutdown in the year 2011. After years of dedication to investigating the Standard Model, one of its most significant achievements was the discovery of the top quark in 1995 [Col95]. The CDF and DO experiments also searched for the Higgs boson. In 2010, these collaborations published results of a combined search for the Higgs boson, using 4.8 fb^{-1} and 5.4 fb^{-1} of data collected at a center of mass energy of 1.96 TeV. The decay mode considered was $H \rightarrow W^+W^-$. With this data, a mass range from 162 to 166 GeV was excluded at 95% confidence level for a Higgs boson. This was the first direct constraint on the Higgs mass beyond that obtained by LEP [Col10]. Recent results from the Tevatron are given in [Col13h] in which an excess of events corresponding to a statistical significance of about 3 standard deviations is reported at a mass of about 125 GeV. This showed evidence of a new particle at that mass.

3.3 Search for the Higgs Boson at ATLAS

After the shutdown of LEP, the LHC began its operation in the year 2008. ATLAS, a general purpose detector of the LHC was one of the detectors that embarked on a journey to search for the Higgs. The Standard Model predicts a number of ways in which the Higgs boson can be produced. At the LHC, the production modes for the Higgs include gluon-gluon fusion (ggF), Vector Boson Fusion (VBF), associative production with a W or Z boson and associative production with a top pair, of which ggF is the dominant production mode. The Feynman diagrams of these production modes are shown in Fig. 3.3. Evaluating the Feynman diagrams using the Feynman rules, gives the scattering amplitude of a particular process, which is then used to evaluate the production cross section, σ, of the Higgs boson via that process. The cross section determines the probability of occurrence of a particular interaction. As an example, Fig. 3.4 (a) shows the Higgs production cross sections, as a function of the Higgs mass, predicted for the 8 TeV center of mass energy at the LHC.

Experiments search for the Higgs boson by analysing its decay products, which are predicted by the Standard Model. Before it's discovery, the Higgs was sought in a wide mass range as the Standard Model made no prediction of its mass. Fig. 3.4 (b) shows the branching ratios[1], as a function of mass, of the Higgs decaying to various particles. The search for the Higgs commences with the collection of events that have specific decay products of the Higgs, for example a pair of photons. The diphoton invariant mass is then calculated from the 4-momentum of the two

[1]Branching ratio gives the probability of a particle decaying through a given process.

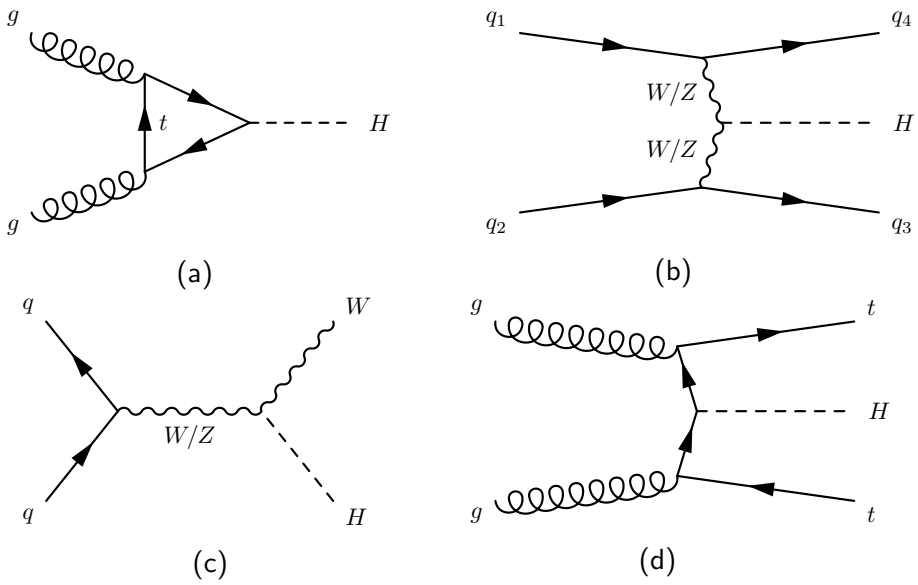

Figure 3.3: Feynmann diagrams of Higgs production modes. Gluon fusion (a), vector boson fusion (b),associative production with W/Z (c) and associative production with a top pair (d) [Ege98]

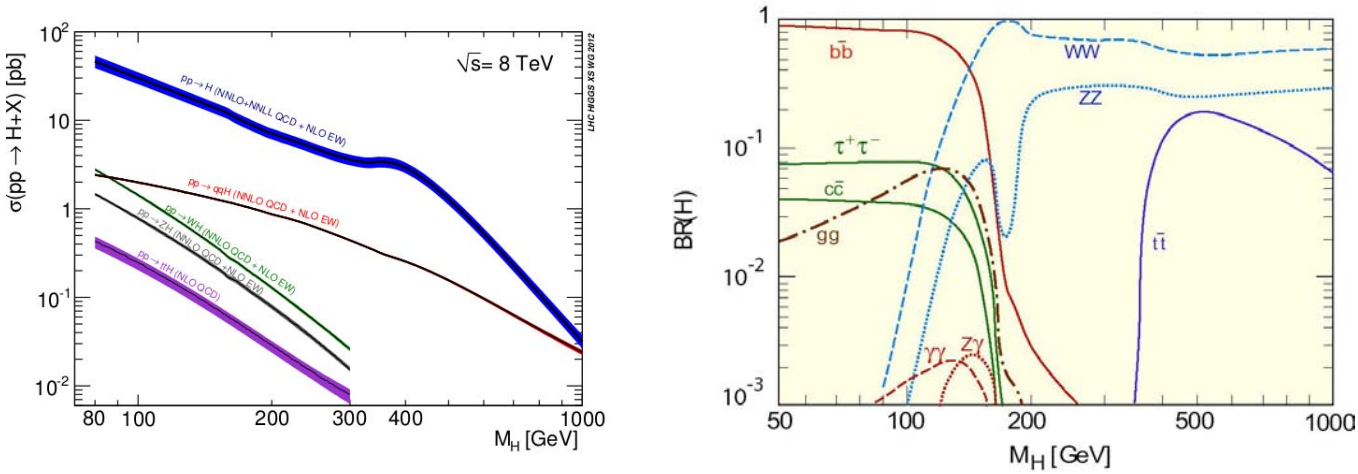

Figure 3.4: (a) Higgs production cross sections as a function of mass at 8 TeV center of mass energies. (b) Higgs decay branching ratios as a function of mass. [cswg13]

photons as shown in Equation 3.3.1, where θ is the opening angle between the two photons.

$$m_{\gamma_1\gamma_2} = \sqrt{2(E_{\gamma_1}E_{\gamma_2}(1-\cos\theta))} \tag{3.3.1}$$

The invariant mass distribution is then plotted. To infer the observation of a particle, one looks for an excess of events on top of a background. Statistical analysis techniques then follow to check if this is a statistically significant signal or not (See Section 3.1). The diphoton decay

channel was one of the best channels in which ATLAS considered the discovery of the Higgs due to its clear signature. In 2011, the ATLAS collaboration published results that showed an excess of events at about 125GeV in the diphoton decay channel [Col11b]. This corresponded to about 2.6 standard deviations and hence did not clearly indicate any evidence of a new particle at that mass. However, when the center of mass energy of proton-proton collisions at the LHC was increased to 8 TeV in 2012, ATLAS discovered a Higgs-like particle at 126 GeV in the combined search for the Higgs using 7 and 8 TeV data [Col12a]. Fig. 3.5 shows the combined p-value plot for all the decay channels considered (ZZ, W^+W^- and $\gamma\gamma$) at both 7 and 8 TeV. A statistical significance of 5.9σ was observed at 126 GeV, hence the discovery. See Section 3.1 for details on p-values and statistical significance.

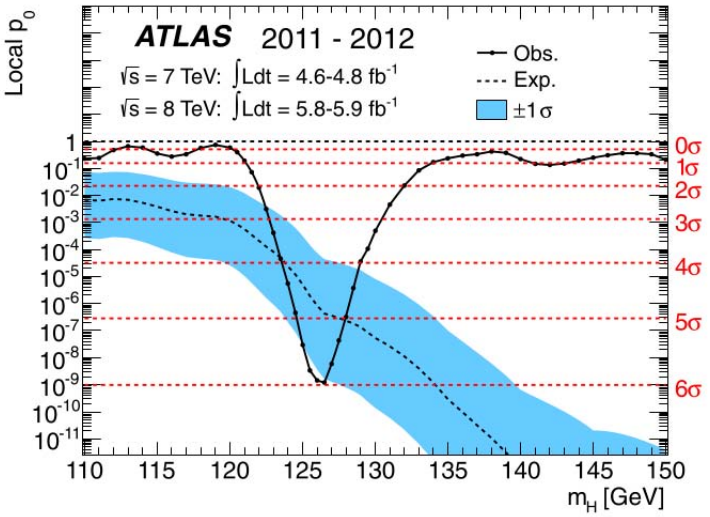

Figure 3.5: The observed (solid) local pvalue (p_0) as a function of m_H in the low mass range. The dashed curve shows the expected local pvalue under the hypothesis of a SM Higgs boson signal at that mass [Col12a].

3.4 Search for an Invisibly Decaying Higgs Boson

Besides the decay channels in which this discovery was established, there are other Higgs decay channels predicted by the Standard Model. These channels have to be explored in order to fully understand the Standard Model. This thesis focuses on one of these channels; the invisible decay channel. While the predicted invisible branching fraction for a Standard Model Higgs boson is too small to be accessible ($\approx 1.2\times10^{-3}$), studies of the invisible decay of the Higgs boson are sensitive to enhancements of the invisible branching fraction such as from decays to dark matter candidates. Therefore, exploring the invisible decay channel of the Higgs could also give

evidence of the existence of exotic particles like dark matter particles. The ATLAS experiment has previously looked at this channel in the ZH production mode of the Higgs, where the Z boson decays to leptons and the Higgs decays invisibly [Col13d]. The results obtained showed no significant excess over the expected background and limits were set on the allowed invisible branching fraction of the recently observed 125 GeV Higgs boson candidate. The upper limit on the observed branching ratio was set at 65% at 95% confidence level. Limits were also set on the cross section×branching ratio of additional Higgs-like particles decaying invisibly in the mass range 115 to 300 GeV. However, no excess was observed. These results are shown in Fig. 3.6.

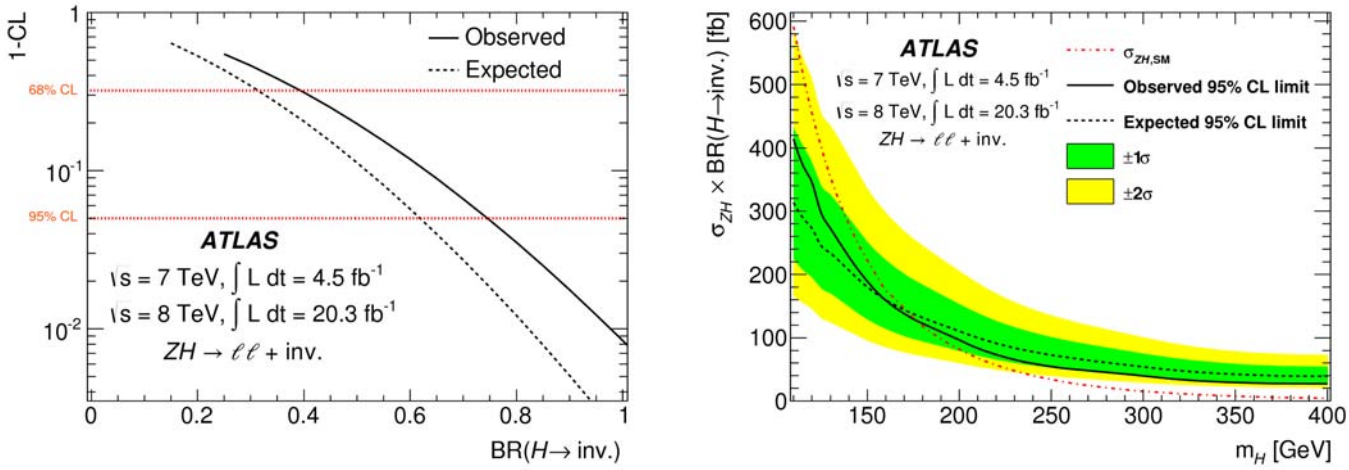

(a) (b)

Figure 3.6: (a) Confidence level (CL) scanned against BR(H→invisible) for the SM Higgs boson at 125 GeV. (b) 95% confidence level limits on the cross section times branching ratio of a Higgs-like particle decaying to invisible particles [Col13d].

The CMS experiment has also conducted a number of searches for the Higgs in the invisible decay mode. In a recent study, CMS observed an upper limit of 75% on the branching ratio of a 125 GeV Higgs to invisible particles in the ZH production mode [Col13g]. This thesis also performs a search for an invisibly decaying Higgs boson at 125 GeV in events with one or two jets plus missing transverse energy. The production modes considered include ggF, VBF and the associative production modes.

4. Methodology

This chapter describes the details of the data used and the analysis strategy followed. All the 7 TeV data presented here and Chapter 5 are "ATLAS Preliminary", while the 8 TeV toy-data presented is "ATLAS work in progress". "ATLAS work in progress" means that the data and results have not yet been officially reviewed by the ATLAS collaboration. "ATLAS preliminary" means that the data and results have been reviewed by the collaboration and have been declared acceptable as public results, but are not yet published in a peer-reviewed scientific journal.

This study used the monojet data which looks for the particular final state of events with a single or a couple of jets plus E_T^{miss} [Col12e], the focus being on events with one or two jets corresponding to Higgs plus 1 jet or Higgs plus 2 jets productions. The study involved setting an upper limit on the branching ratio, to invisible particles, of the Higgs-like boson at 125 GeV and on the cross section times branching ratio of additional Higgs-like particles that decay invisibly in the mass range 115 to 300 GeV. This study corresponds to 4.7 fb^{-1} of 7 TeV proton-proton collisions and 20.3 fb^{-1} of 8 TeV proton-proton collisions. At the time of thesis submission, the 8 TeV results were not unblinded by the ATLAS Collaboration, therefore, toy-data are presented here to demonstrate the procedure. This was done to study the behaviour of the statistical framework to be used in the combination of the 7 TeV and 8 TeV data once the real 8 TeV data becomes un-blinded. Consequently, only the results using the 7 TeV data are meaningful, the results obtained using 8 TeV data can not be used to draw a physical conclusion.

The production mechanisms for the Higgs that were searched for in this study consisted of ggF (with one or two jets from radiation), VBF[1] and the associated production mechanisms: ZH and WH where Z/W$\rightarrow \mathrm{q\bar{q}}$. The signal events at both 7 and 8 TeV were modelled using Powheg MonteCarlo (MC) event generator [ea09b], [NO10]. Background contributions from other Standard Model processes were expected to result from the following processes; Z($\nu\nu$)+jets, W($\tau\nu$), W($e\nu$)+jets, W($\mu\nu$)+jets, Z($\tau\tau$)+jets, Z($\mu\mu$)+jets, Z(ee)+jets, Multi-jets, $t\bar{t}$+single t, Di-bosons and Non-collision backgrounds. The $t\bar{t}$+single t and Di-bosons backgrounds were estimated from Monte Carlo whereas the rest were estimated from the data.

Section 4.1 describes the event selection criteria used for jets and E_T^{miss} and highlights the signal, background and data inputs used in the analysis at both 7 TeV and 8 TeV. Finally, section 4.2 discusses the implementation of the statistical analysis techniques for limit setting used in the data analysis. The work described in Section 4.1 was done by the monojet group at ATLAS,

[1] In VBF, two vector bosons are radiated from quarks coming from a p-p collision and their interaction produces a Higgs.

where as this thesis work is described in Section 4.2.

4.1 Data Inputs at 7 and 8 TeV

To achieve a high level of sensitivity to an invisibly decaying Higgs, three categories of data were used in this analysis. The first category included the 7 TeV data which had events with either one or two jets plus E_T^{miss}. The second category included the 8 TeV 1−jet data which had events with only one jet plus E_T^{miss}. Finally, the third category included the 8 TeV 2−jet data which had events with strictly two jets plus E_T^{miss}. Furthermore, each category was separated into various signal regions defined with increasing lower threshold on E_T^{miss}. The basic selection of events at both 7 and 8 TeV followed the requirements given in [Col12d]. In addition to this, the following selection criteria were also applied.

- The p_T of the leading jet was required to be above 120 GeV where as the E_T^{miss} was scanned in increasing values from 150 GeV in steps of 50 GeV to define the various signal regions as shown in Tables 4.1, 4.2 and 4.3.
- In order to suppress non-collision backgrounds, the magnitude of the pseudorapidity of the leading jet was required to be less than 2 (i.e $|\eta|$ <2).
- The $\triangle\phi$ for any jet or E_T^{miss} was required to be greater than 2.2 in order to suppress dijet events from the backgrounds.
- For the associated production, the dijet invariant mass, $\mathrm{m_{jj}}$, was required to be consistent with $\mathrm{m_Z}$ or $\mathrm{m_W}$.
- For VBF events, $\mathrm{m_{jj}}$ was required to be in the range 500< $\mathrm{m_{jj}}$ <1000 GeV.
- The p_T of the subleading (second highest p_T) jet was required to be greater than 30 GeV.

The 7 TeV category was separated into four signal regions. These included signal region one (SR1), signal region two (SR2), signal region three (SR3) and signal region four (SR4). Each of the 8 TeV categories were separated into three signal regions; signal region one (SR1), signal region three (SR3) and signal region five (SR5). Tables 4.1, 4.2 and 4.3 respectively show the 7 TeV, 8 TeV 1−jet and 8 TeV 2−jet signal regions with the E_T^{miss} cuts imposed on them. In each category, each signal region was analysed independently. In addition, this was done for each of

Signal Region	minimum E_T^{miss} (GeV)
SR1	150
SR2	200
SR3	250
SR4	300

Table 4.1: Definition of the 7 TeV signal regions.

Signal Region	minimum E_T^{miss} (GeV)
SR1	150
SR3	250
SR5	350

Table 4.2: Definition of the 8 TeV 1−jet signal regions.

Signal Region	minimum E_T^{miss} (GeV)
SR1	150
SR3	250
SR5	350

Table 4.3: Definition of the 8 TeV 2−jet signal regions.

the following masses; 115, 120, 125, 130, 150, 200 and 300 GeV. In what follows, the analysis procedure is illustrated using SR1 of the 7 TeV data at 125 GeV.

The expected signal yields, N, from ggF, VBF, WH and ZH production modes were evaluated using Equation 4.1.1. The luminosity and BR used for a 125 GeV Higgs in SR1 (7 TeV) were 4.7 fb^{-1} and 1.0 respectively. The Acceptance×Efficiency for each production mode is shown in Table 4.4. The production cross sections are shown in Table 4.5.

Mode	Acceptance×Efficiency
ggF	2.508%
VBF	6.296%
WH	5.575%
ZH	5.387%

Table 4.4: Acceptance×Efficiency used for the 125 GeV Higgs in SR1 (7 TeV).

$$\mathrm{N} = \mathrm{Luminosity} \times \sigma \times \mathrm{BR} \times \mathrm{Acceptance} \times \mathrm{Efficiency} \tag{4.1.1}$$

Expected backgrounds were estimated from data-driven techniques and Monte Carlo techniques

Signal Process (m_H = 125 GeV)	σ [pb] (7 TeV)
ggF	$15.13^{+7.1\%+7.6\%}_{-7.8\%-7.1\%}$
VBF	$1.222^{+0.3\%+2.5\%}_{-0.3\%-2.1\%}$
WH	$0.5787^{+0.9\%+2.6\%}_{-0.9\%-2.6\%}$
ZH	$0.3351^{+2.9\%+2.7\%}_{-2.9\%-2.7\%}$

Table 4.5: Production Cross sections for a 125 GeV Higgs at 7 TeV. The uncertainties shown represent QCD effects (first) and PDF (Parton distribution function) effects (second).

as explained at the beginning of this chapter. The data has statistical uncertainties and is affected by systematic uncertainties. Theoretical systematic uncertainties included the Higgs p_T shape uncertainties and renormalization and factorization scales (QCD scales) and PDF+α_s uncertainties on the total cross sections for the signal. QCD and PDF+α_s uncertainties are shown in Table 4.5. Theoretical systematic uncertainties only affect the signal. Detector systematic uncertainties included:

- Jet Energy Scale uncertainty (JES): This is an uncertainty in the determination of jet energies and it affects all expected signal and backgrounds.
- MC background subtraction (Bkg Sub): This arises from the control regions used for data-driven backgrounds and only affects data-driven backgrounds.
- Shape uncertainty: This arises from the Z/W+jets background modelling determined by using SHERPA [ea04] instead of ALPGEN [ea03b] in the simulation of MC samples. It affects data driven backgrounds.
- Lepton Identification Efficiency (LEPID): This affects signal and non data driven backgrounds.
- Uncertainty in the luminosity: This affects all signal and non datadriven backgrounds.

The observed data, expected signal and background yields as well as their associated statistical uncertainties used for a 125 GeV Higgs in SR1 (7 TeV) are shown in Table 4.6. Theoretical and detector systematic uncertainties are shown in Table 4.7. These tables contain all the information required to set branching ratio (H$\rightarrow \nu\nu$) upper limits on a 125 GeV Higgs boson in SR1 at 7 TeV. With this information in place, the statistical techniques for limit setting were implemented as explained in Section 4.2.

Process	Yield	Data Statistics	MC Statistics
ggF125	1783	–	$\pm$42
VBF125	361	–	$\pm$19
WH125	101	–	$\pm$10
ZH125	58	–	$\pm$7
Z($\nu\nu$)+jets	63000	$\pm$279	$\pm$270
W($\tau\nu$)+jets	31400	$\pm$138	$\pm$159
W($e\nu$)+jets	14600	$\pm$121	$\pm$89
W($\mu\nu$)+jets	11100	$\pm$50	$\pm$101
Z($\tau\tau$)+jets	421	$\pm$4	$\pm$10
Z($\mu\mu$)+jets	204	$\pm$2	$\pm$15
Multijets	1100	$\pm$33	–
$t\bar{t}$+single t	1240	–	11
Dibosons	302	–	$\pm$3
Non-collision	575	$\pm$60	–
Data	124703	–	–

Table 4.6: Number of observed data events and expected background events with their statistical uncertainties in SR1 (7 TeV) at 125 GeV .

4.2 Implementation of Statistical Techniques

Statistical analysis proceeded with the creation of the binned marked Poisson statistical model described in Section 3.1.1, but with a single bin. This was implemented using the Histfactory statistical package [ea12]. The Histfactory tool uses a statistical framework known as ROOFit [WV08] to build parametrized probability density functions based on single bin histograms organized in an XML file. The XML file takes as input, the single bin histograms of the data, expected signal yields and background yields. The systematic uncertainties associated with each signal and background are also added to the XML file and the parameter of interest is also specified as μ. An XML with these inputs is known as a channel XML. The channel XML for a 125 GeV Higgs in SR1 (7 TeV) is shown in Appendix A. This channel XML is executed from the combination XML also shown in Appendix A. Once the combination XML is executed, the resulting statistical model, containing all the information necessary for statistical tests, is stored in a workspace called RooWorkspace.

The limits are computed from a maximum likelihood fit to the data, following the CL_s technique and the profile likelihood test statistic for limit setting as described in Section 3.1.3. This is

Process	QCDscale	PDF+α_s	Higgs P_T	JES	Bkg Sub	Shape	LEPID	Lumi
ggF125	$^{+0.07}_{-0.08}$	$^{+0.08}_{-0.07}$	$^{+0.10}_{-0.10}$					
VBF125	± 0.003	$^{+0.03}_{-0.02}$	± 0.08	± 0.03	–	–	± 0.08	± 0.039
WH125	± 0.01	± 0.03	± 0.12	± 0.04	–	–	± 0.08	± 0.039
ZH125	± 0.03	± 0.03	± 0.08	± 0.04	–	–	± 0.08	± 0.039
Z($\nu\nu$)+jets	–	–	–	± 0.015	± 0.01	± 0.03	–	–
W($\tau\nu$)+jets	–	–	–	± 0.015	± 0.01	± 0.03	–	–
W($e\nu$)+jets	–	–	–	± 0.015	± 0.01	± 0.03	–	–
W($\mu\nu$)+jets	–	–	–	± 0.015	± 0.01	± 0.03	–	–
Z($\tau\tau$)+jets	–	–	–	± 0.015	± 0.01	± 0.03	–	–
Z($\mu\mu$)+jets	–	–	–	± 0.015	± 0.01	± 0.03	–	–
Multijets	–	–	–	± 0.015	± 0.01	± 0.03	–	–
$t\bar{t}$+single t	–	–	–	± 0.015	–	–	± 0.008	± 0.039
Dibosons	–	–	–	± 0.015	–	–	± 0.008	± 0.039
Non-collision	–	–	–	± 0.015	± 0.01	± 0.03	–	–

Table 4.7: Theoretical and detector systematic uncertainties in SR1 (7 TeV) at 125 GeV .

implemented using the ROOStats statistical package [ea09a]. To set limits, RooStats performs an inverted hypothesis test on the data, such that the null hypothesis is taken to be the background-only hypothesis and the signal+background hypothesis is taken to be the alternative hypothesis. To set an upper limit on μ, μ values in the range 0.1 to 3.0 were scanned. The confidence level used was 95% such that the highest μ value in the set of μ values with p-values greater than 1-0.05, was considered the upper limit.

For each signal region described in Section 4.1, the above procedure was followed for each possible Higgs mass. Since all branching ratios for the expected signal were set to 1.0, the upper limit on μ was interpreted as an upper limit on the branching ratio, to invisible particles, of a 125 GeV Higgs. To get the upper limits for the full mass range considered, μ was multiplied by the total production cross section from ggF, VBF, WH and ZH. It was then interpreted as an upper limit on the production cross section×Branching ratio of a Higgs-like particle at a particular mass. Both the expected and observed upper limits were estimated. To get the final result, the signal regions with the tightest expected upper limits, based on the 125 GeV Higgs, in each category were combined. Results are shown in Chapter 5 below.

5. Results

This chapter presents the results obtained from all the categories and their combination. Section 5.1 presents results obtained from the 7 TeV category. Sections 5.2 and 5.3 present results obtained from the 8 TeV 1-jet and 2-jet categories respectively. Finally, section 5.4 presents results obtained from the combination of the best signal regions in each category. All results are quoted at 95%CL though the 68%CL limit is also shown. In each category, the expected 95%CL upper limits exceed 1.00 which implies that the measurements are not sensitive enough to be interpreted as upper limits on the branching ratio. Therefore, for a 125 GeV Higgs, the results are interpreted as limits on the ratio of the production cross section $\times$ branching ratio to the SM cross section ($\sigma\times$BR/σ_{SM}). However, in the combination of the three categories, the upper limits do not exceed 1.00 and can thus be interpreted as branching ratio upper limits, except at 300 GeV. In the full mass range, upper limits are set on the production cross section$\times$Branching ratio and no deviation from the SM expectation is noted in either of the categories and their combination.

All results presented in each category are referred to as "ATLAS work in progress" results (refer to the beginning of Chapter 4).

5.1 Results at 7 TeV

Results obtained from the 7 TeV category are shown in Tables 5.1, 5.2, 5.3 and 5.4. These tables show the expected and observed upper limits for the entire mass range studied in SR1, SR2, SR3 and SR4 respectively. Fig 5.1 shows the limit plots on the $\sigma\times$BR/σ_{SM} of a 125 GeV Higgs for all the 7 TeV signal regions and Fig 5.2 shows the upper limit plots on the cross-section$\times$BR for the entire mass range. σ_{tot} represents the total SM production cross sections from the ggF, VBF, WH and ZH production modes. The expected (observed) upper limits on $\sigma\times$BR/σ_{SM} of a 125 GeV Higgs were found to be; 2.65 (2.41) for SR1, 1.38 (1.56) for SR2, 1.96 (1.44) for SR3 and 1.60 (1.92) for SR4. Based on the expected upper limits, the signal region with the tightest limit is SR3.

Mass	ObservedCLs	ExpectedCLs	−1sig	+1sig	−2sig	+2sig
115	2.53	2.29	1.64	3.16	1.24	3.82
120	2.63	2.39	1.70	3.25	1.28	3.95
125	2.65	2.41	1.72	3.26	1.29	3.98
130	2.80	2.55	1.83	3.36	1.34	4.14
150	3.00	2.74	1.96	3.52	1.48	4.43
200	3.76	3.56	2.81	4.45	2.09	6.79
300	4.88	4.53	3.71	6.36	3.08	13.07

Table 5.1: SR1 Limits at all mass points at 7 TeV

Mass	Observed CLs	Expected CLs	-1sig	+1sig	-2sig	+2sig
115	1.31	1.50	1.07	2.10	0.83	2.90
120	1.50	1.65	1.21	2.34	0.91	3.16
125	1.38	1.56	1.13	2.21	0.86	3.03
130	1.52	1.66	1.22	2.40	0.92	3.21
150	1.35	1.55	1.11	2.19	0.85	3.01
200	1.86	2.08	1.50	2.95	1.12	3.61
300	2.24	2.51	1.80	3.35	1.32	4.12

Table 5.2: SR2 Limits

Mass	Observed CLs	Expected CLs	-1sig	+1sig	-2sig	+2sig
115	2.17	1.58	1.11	2.29	0.84	3.22
120	2.23	1.62	1.16	2.34	0.88	3.24
125	1.95	1.43	0.99	2.06	0.77	2.95
130	2.36	1.72	1.23	2.52	0.92	3.37
150	1.98	1.46	1.01	2.11	0.79	3.00
200	2.54	1.85	1.30	2.67	0.96	3.49
300	2.60	1.89	1.32	2.73	0.98	3.51

Table 5.3: SR3 Limits

Mass	Observed CLs	Expected CLs	-1sig	+1sig	-2sig	+2sig
115	1.65	1.99	1.29	3.24	0.94	4.27
120	2.61	3.14	1.94	4.27	1.32	6.15
125	1.61	1.94	1.29	3.11	0.94	4.07
130	1.55	1.86	1.23	3.02	0.90	4.01
150	1.77	2.14	1.37	3.39	0.97	4.45
200	2.53	3.06	1.93	4.13	1.33	5.82
300	1.91	2.30	1.53	3.46	1.09	4.49

Table 5.4: SR4 Limits

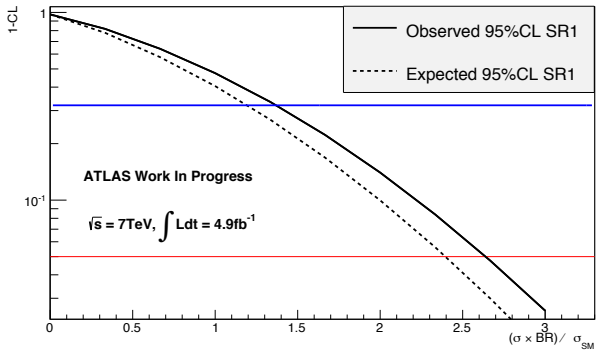

(a) SR1

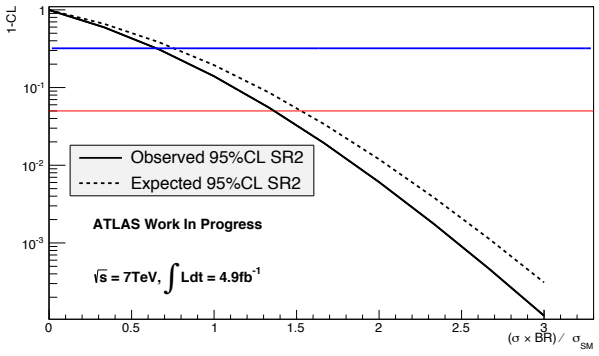

(b) SR2

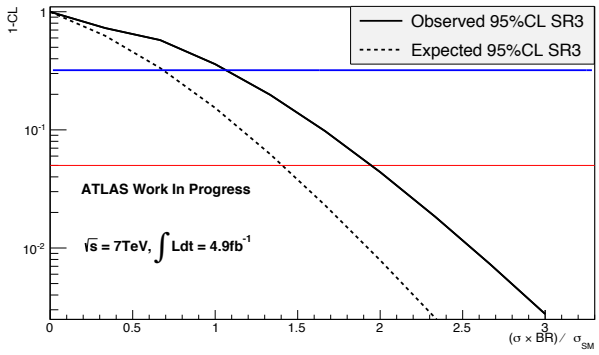

(c) SR3

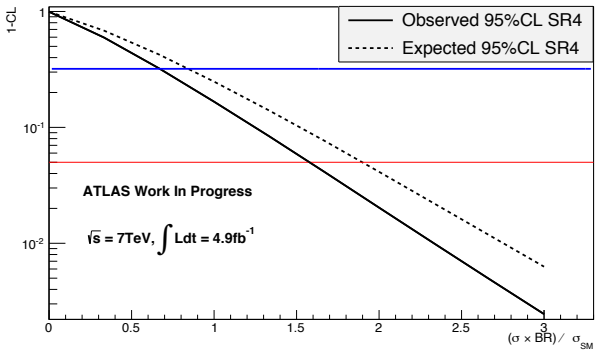

(d) SR4

Figure 5.1: Observed and expected confidence level limits on the ($\sigma \times$BR(H $\rightarrow$ invisible)/σ_{SM}) of a 125 GeV Higgs boson in the 7 TeV category for all signal regions considered. The blue solid line indicates a 1-68%CL and the red solid line indicates a 1-95%CL.

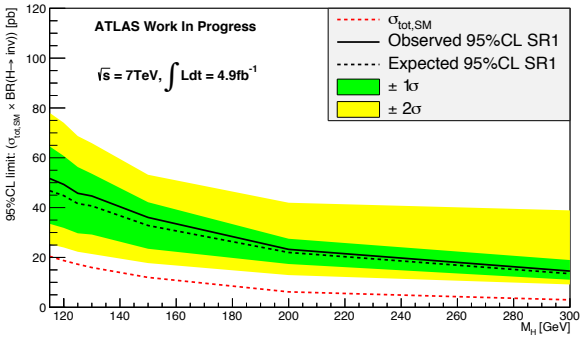

(a) SR1

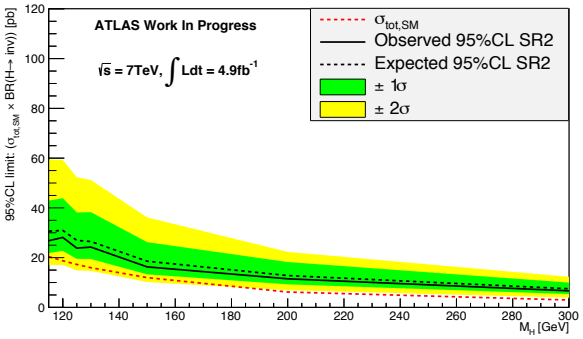

(b) SR2

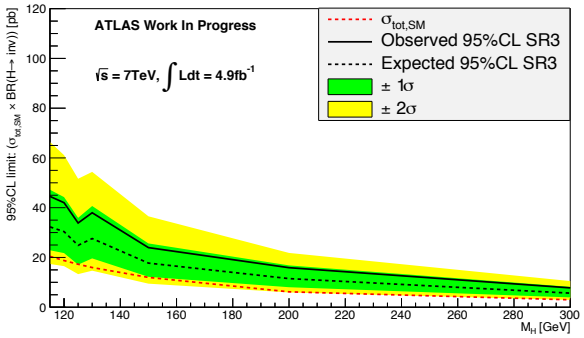

(c) SR3

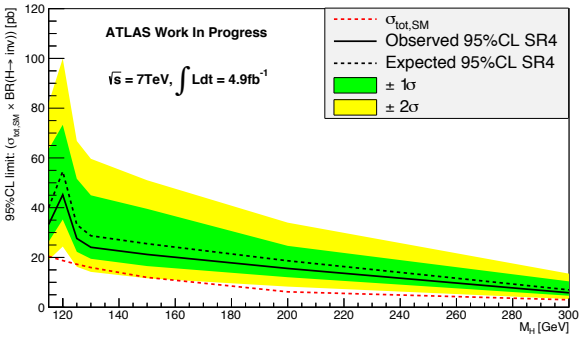

(d) SR4

Figure 5.2: 95%CL upper limits on the cross section×branching ratio of a Higgs-like particle decaying to invisible particles in the mass range 115 to 300 GeV at $\sqrt{s}$ =7 TeV.

5.2 Results at 8 TeV 1-jet category

Tables 5.5, 5.6 and 5.7 show the 8 TeV 1-jet upper limits and Fig 5.3 shows their plots. The left panel shows the limit plots for a 125 GeV Higgs and the right panel shows the limit plots for the entire mass range. The expected (observed) upper limits for a 125 GeV Higgs are found to be 1.68 (0.66) in SR1, 2.16 (2.00) in SR3 and 2.26 (2.18) in SR5. The best signal region is considered to be SR1 and no excess over the SM expectation is observed in the full mass range.

Mass	ObservedCLs	ExpectedCLs	−1sig	+1sig	−2sig	+2sig
115	0.66	1.66	1.21	2.19	0.89	2.66
120	0.64	1.58	1.14	2.13	0.86	2.56
125	0.66	1.68	1.22	2.20	0.90	2.68
130	0.71	1.77	1.29	2.28	0.97	2.82
150	0.75	1.86	1.33	2.34	1.01	2.95
200	1.01	2.33	1.83	2.89	1.36	4.32
300	1.52	3.02	2.47	4.23	2.06	8.70

Table 5.5: SR1 Limits at all mass points at 8 TeV 1-jet

Mass	Observed CLs	Expected CLs	-1sig	+1sig	-2sig	+2sig
115	1.77	1.89	1.35	2.61	1.01	3.29
120	1.93	2.04	1.50	2.85	1.13	3.47
125	2.00	2.16	1.57	2.98	1.19	3.58
130	2.15	2.28	1.64	3.11	1.25	3.73
150	2.56	2.72	1.97	3.48	1.49	4.34
200	2.74	2.92	2.12	3.63	1.59	4.66
300	3.70	3.84	3.16	4.95	2.40	8.30

Table 5.6: SR3 Limits at 8 TeV 1-jet

Mass	Observed CLs	Expected CLs	-1sig	+1sig	-2sig	+2sig
115	1.97	2.05	1.49	2.88	1.12	3.53
120	2.01	2.10	1.53	2.94	1.15	3.57
125	2.18	2.26	1.62	3.12	1.23	3.77
130	1.72	1.80	1.29	2.51	0.97	3.25
150	1.95	2.02	1.48	2.85	1.11	3.50
200	2.99	3.08	2.23	3.81	1.65	5.08
300	3.18	3.26	2.41	4.02	1.81	5.60

Table 5.7: SR5 Limits at 8 TeV 1-jet

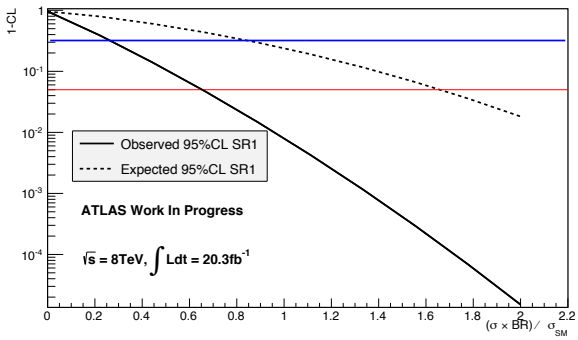

(a) SR1

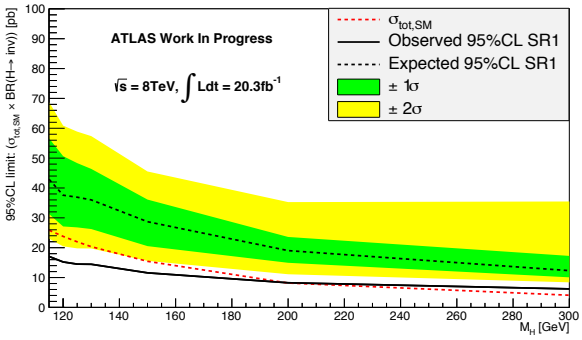

(b) SR1

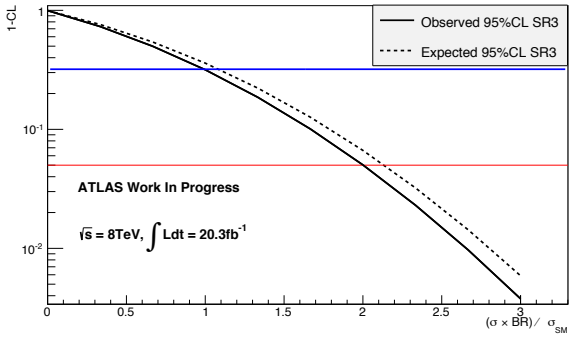

(c) SR3

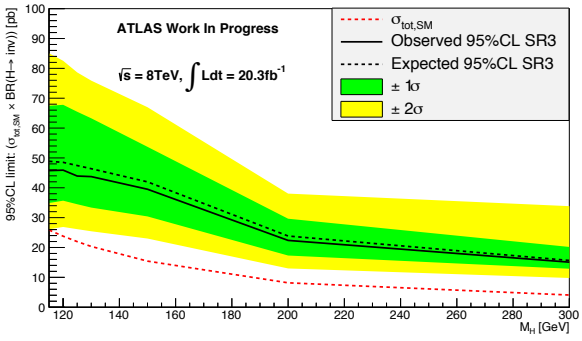

(d) SR3

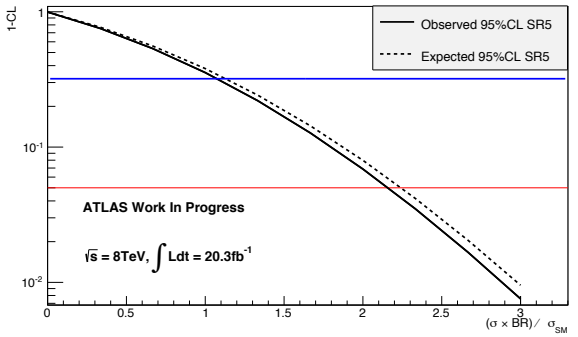

(e) SR5

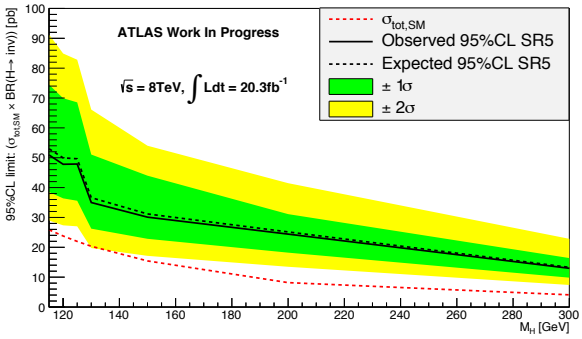

(f) SR5

Figure 5.3: [$\sqrt{s}$ =8 TeV (1-jet category)] Left panel: Observed and expected confidence level limits on the ($\sigma \times$BR(H $\rightarrow$ invisible)/σ_{SM}) of a 125 GeV Higgs boson. The blue solid line indicates 1-68%CL and the red solid line indicates 1-95%CL. Right panel: 95%CL upper limits on the cross section$\times$branching ratio of a Higgs-like particle decaying to invisible particles in the mass range 115 to 300 GeV.

5.3 Results at 8 TeV 2-jet category

Results obtained from the study in the 2-jet category are shown in Tables 5.8, 5.9 and 5.10. Fig 5.4 then shows the plots of these results. The expected (observed) upper limits for a 125 GeV Higgs are 1.09 (0.35) in SR1, 1.05 (0.83) in SR3 and 1.40 (0.74) in SR5. According to these results, the best signal region is considered to be SR3. Similar to the other categories, no excess beyond the SM expectation is observed in the mass range 115 GeV to 300 GeV.

Mass	ObservedCLs	ExpectedCLs	−1sig	+1sig	−2sig	+2sig
115	0.30	0.97	0.70	1.20	0.52	1.54
120	0.34	1.08	0.81	1.32	0.61	1.83
125	0.35	1.09	0.82	1.34	0.62	1.87
130	0.34	1.08	0.80	1.32	0.60	1.82
150	0.43	1.23	1.00	1.56	0.75	2.50
200	0.54	1.43	1.18	1.95	0.96	3.75
300	0.99	2.22	1.66	3.80	1.39	11.08

Table 5.8: SR1 Limits at all mass points at 8 TeV 2-jet

Mass	Observed CLs	Expected CLs	-1sig	+1sig	-2sig	+2sig
115	0.64	0.82	0.60	1.12	0.43	1.53
120	0.89	1.13	0.83	1.60	0.62	2.11
125	0.83	1.05	0.76	1.46	0.58	1.98
130	0.78	0.97	0.69	1.34	0.54	1.84
150	1.05	1.32	0.95	1.86	0.71	2.31
200	1.10	1.40	1.01	1.97	0.76	2.40
300	2.15	2.47	1.98	3.13	1.48	4.99

Table 5.9: SR3 Limits at 8TeV 2-jet

Mass	Observed CLs	Expected CLs	-1sig	+1sig	-2sig	+2sig
115	0.38	0.64	0.44	0.88	0.38	1.25
120	0.67	1.29	0.91	1.88	0.67	2.38
125	0.74	1.40	0.99	2.03	0.74	2.51
130	0.81	1.53	1.08	2.16	0.81	2.66
150	0.58	1.07	0.77	1.53	0.58	2.12
200	0.95	1.81	1.27	2.39	0.93	3.07
300	1.54	2.54	2.02	3.28	1.48	5.41

Table 5.10: SR5 Limits at 8TeV 2-jet

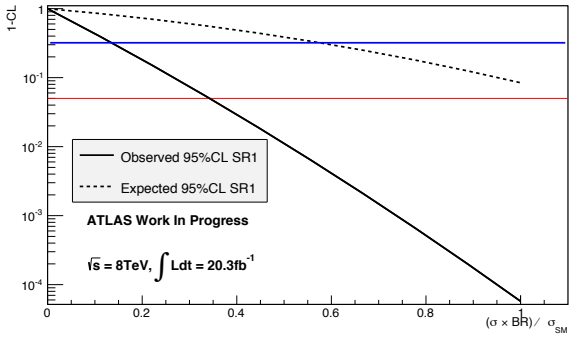

(a) SR1

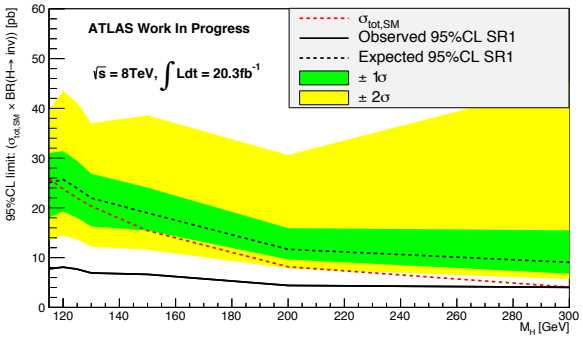

(b) SR1

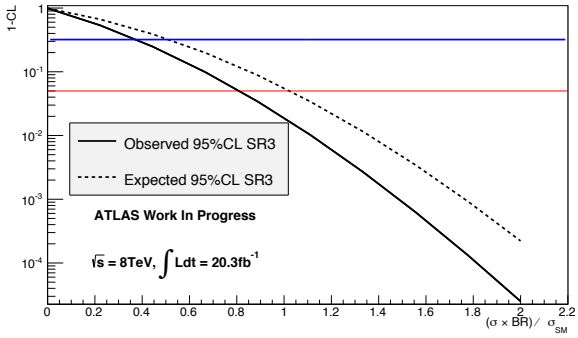

(c) SR3

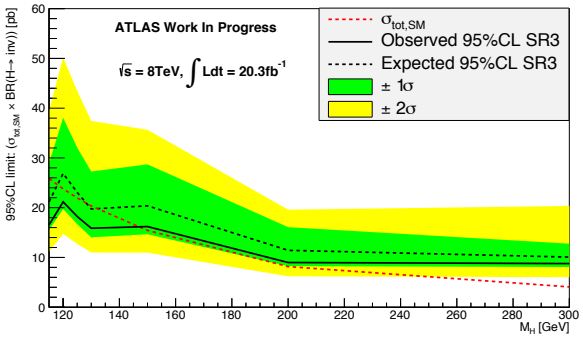

(d) SR3

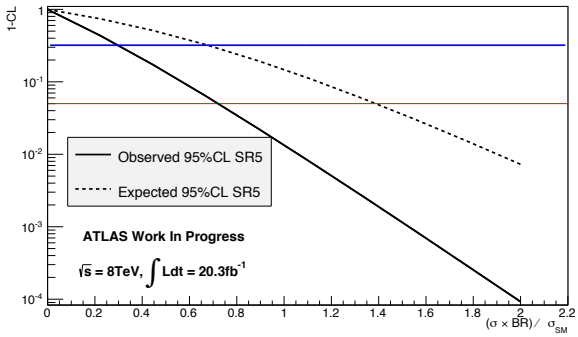

(e) SR5

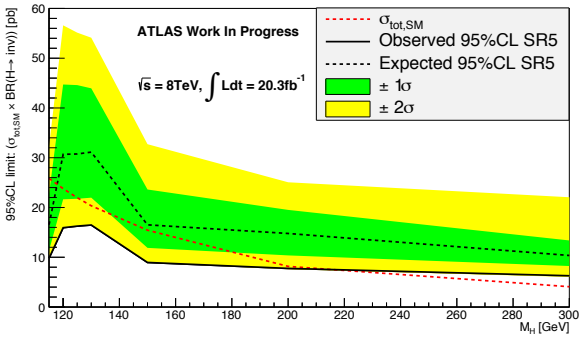

(f) SR5

Figure 5.4: [$\sqrt{s}$ =8 TeV (2-jet category)] Left panel: Observed and expected confidence level limits on the ($\sigma\times$BR(H $\rightarrow$ invisible)/σ_{SM}) of a 125 GeV Higgs boson. The blue solid line indicates 1-68%CL and the red solid line indicates 1-95%CL. Right panel: 95%CL upper limits on the cross section$\times$branching ratio of a Higgs-like particle decaying to invisible particles in the mass range 115 to 300 GeV.

5.4 Combined 7 TeV and 8 TeV Results

Finally, a combination of signal regions SR3 (7TeV), SR1 (8 TeV 1-jet) and SR3 (8 teV 2-jet) give an expected (observed) upper limit of 0.89 (0.59) on the branching ratio of a 125 GeV Higgs boson. Table 5.11 shows the upper limits obtained at all mass points in this combination. Fig 5.5 shows the combined 95%CL limit plot on the branching ratio of a Higgs decaying invisibly at 125 GeV. Fig 5.6 shows the combined 95%CL limit plot on the production cross section×branching ratio of any Higgs-like particle decaying to invisible particles in the mass range 115 to 300 GeV. However, no deviation beyond the SM expectation is observed.

Mass	Observed CLs	Expected CLs	-1sig	+1sig	-2sig	+2sig
115	0.54	0.76	0.59	1.00	0.45	1.36
120	0.58	0.93	0.65	1.27	0.56	1.67
125	0.59	0.89	0.63	1.21	0.53	1.60
130	0.61	0.94	0.65	1.26	0.58	1.71
150	0.65	0.98	0.71	1.35	0.59	1.86
200	0.81	1.18	0.87	1.61	0.64	2.18
300	1.30	1.61	1.18	2.28	0.89	3.08

Table 5.11: Combined 7 and 8 TeV Limits

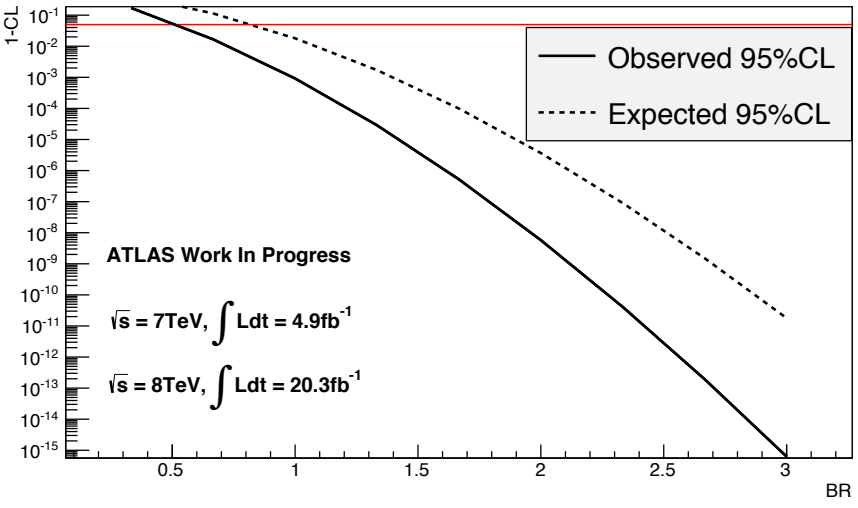

Figure 5.5: The observed and expected 95% confidence level limits on on the Branching ratio for the combined search of an invisibly decaying 125 GeV Higgs.

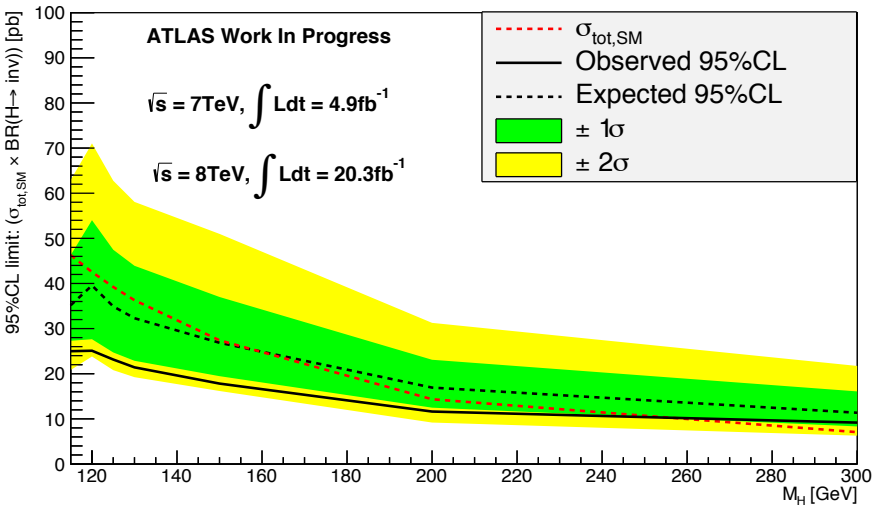

Figure 5.6: The observed and expected 95% confidence level limits on the cross section $\times$ Branching ratio for the combined search of an invisibly decaying Higgs-like particle in the mass range 115 GeV to 300 GeV.

Summary and Conclusion

This study has performed a search for a 125 GeV SM Higgs boson that decays to invisible particles. It has also searched for other Higgs-like particles that could decay to invisible particles in the mass range 115 GeV to 300 GeV. 4.7 fb^{-1} of ATLAS monojet data taken at $\sqrt{s}$ =7 TeV and 20.3 fb^{-1} of toy-data at $\sqrt{s}$ =8 TeV has been used. The data were separated into three categories; the 7 TeV category, the 8 TeV 1-jet category and the 8 TeV 2-jet category. Each of these categories is studied independently before they are combined to give the final result. In the combined result, including the 8 TeV toy-data, the expected (observed) exclusion is for branching ratios (H$\rightarrow vv$) greater than 89$\%$ (59$\%$). In addition, upper limits set on the cross-section$\times$ invisible branching ratio of any Higgs-like particle in the mass range 115 to 300 GeV have indicated no deviation from the Standard Model expectation. The observed 59$\%$ upper limit on the branching ratio to invisible particles achieved in this thesis is a competitive upper bound from events with one or two jets plus missing transverse energy and would provide a significant contribution to the overall combination with similar ATLAS search results, leading to a much tighter ATLAS combined limit. However, it is important to note that toy-data was used at 8 TeV, so the result is not physically meaningful. Once the 8 TeV data becomes un-blinded, they will be employed in this analysis to produce a physically meaningful result. This study has shown that this statistical framework behaves well in the combination of the various categories and is ready for use once the real 8 TeV data is available.

Bibliography

[Ali12] John Alison, *The road to discovery: Detector alignment,electron identification, particle misidentification, WW physics, and the discovery of the Higgs boson*, PhD thesis, University of Pennsylvania (2012).

[Bet08] Alessandro Bettini, *Introduction to elementary particle physics*, Cambridge University press, 2008.

[Cas11] Diego Casadei, *Statistical methods used in ATLAS for exclusion and discovery*, arXiv:1108.2288v1 (2011).

[Col95] CDF Collaboration, *Observation of top quark production in pp collisions*, arXiv:hep-ex/9503002v2 (1995).

[Col99] ATLAS Collaboration, *ATLAS detector and physics performance, technical design report*, ATLAS TDR 15, CERN/LHCC 99-15 **2** (1999).

[Col08a] ALICE Collaboration, *The ALICE experiment at the CERN LHC s08002*, JINST **3** (2008).

[Col08b] ATLAS Collaboration, *The ATLAS experiment at the CERN Large Hadron Collider s08003*, JINST **3** (2008).

[Col08c] ———, *Expected performance of the ATLAS experiment; detector, trigger and physic*, CERN-OPEN-2008-020 (2008).

[Col08d] CMS Collaboration, *The CMS experiment at the CERN LHC s08004*, JINST **3** (2008).

[Col08e] LHCb Collaboration, *The LHCb experiment at the CERN LHC s08005*, JINST **3** (2008).

[Col08f] LHCf Collaboration, *The LHCf experiment at the CERN LHC s08006*, JINST **3** (2008).

[Col08g] TOTEM Collaboration, *The TOTEM experiment at the CERN LHC s08007*, JINST **3** (2008).

[Col10] FERMILAB Collaboration, *Combination of Tevatron searches for the Standard Model Higgs boson in the WW decay mode*, FERMILAB-PUB-10-017-E (2010).

[Col11a] ATLAS Collaboration, *Measurement of the W+W−; production cross section in p-p collisions at $\sqrt{s}$ =7 tev with the ATLAS detector*, ATLAS-CONF-2011-015 (2011).

[Col11b] ———, *Search for the Standard Model Higgs boson in the diphoton decay channel with 4.9 fb^{-1} of ATLAS data at $\sqrt{s}$ =7 tev*, ATLAS NOTE, 2011.

[Col12a] _____, *Observation of a new particle in the search for the Standard Model Higgs boson with the ATLAS detector at the LHC*, Physics Letters B **716** (2012).

[Col12b] _____, *Observation of an excess of events in the search for the Standard Model Higgs boson in the gamma-gamma channel with the ATLAS detector*, ATLAS-CONF-2012-091 (2012).

[Col12c] _____, *A particle consistent with the Higgs boson observed with the ATLAS detector at the Large Hadron Collider*, Science **338** (2012).

[Col12d] _____, *Search for dark matter candidates and large extra dimensions in events with a jet and missing transverse momentum with the ATLAS detector*, arXiv:1210.4491v2 (2012).

[Col12e] _____, *Search for new phenomena in monojet plus missing transverse momentum final states using 10 fb*^{1} *of pp collisions at* $\sqrt{s}$*=8 tev of* pp *collisions with the ATLAS detector at the LHC*, ATL-CONF-2012-147 (2012).

[Col12f] CMS Collaboration, *Observation of a new boson at a mass of 125 gev with the CMS experiment at the LHC*, Physics Letters B **716** (2012).

[Col13a] ATLAS Collaboration, *Combined coupling measurements of the Higgs-like boson with the ATLAS detector using up to 25 inverse fb of proton-proton collision data*, Tech. Rep. ATLAS-CONF-2013-034 (2013).

[col13b] ATLAS collaboration, *Jet energy measurement with the ATLAS detector in proton-proton collisions at 7 tev*, Eur.Phys.J.C 73:2304 (2013).

[Col13c] ATLAS Collaboration, *Search for invisible decays of a Higgs boson produced in association with a Z boson in ATLAS*, Tech. Rep. ATLAS-CONF-2013-011 (2013).

[Col13d] _____, *Search for invisible decays of a Higgs boson produced in association with a Zboson in ATLAS*, arXiv:1402.3244 (2013).

[Col13e] _____, *Study of the spin of the Higgs-like boson in the two photon decay channel using 20.7 fb*^{1} *of pp collisions collected at* $sqrts = 8$ *tev with the ATLAS detector*, ATLAS NOTE, 2013.

[Col13f] _____, *Study of the spin properties of the Higgs-like boson in the H*$\rightarrow ww^{(*)} \rightarrow ev\mu v$ *channel with 21 fb*^{1} *of* $sqrts$ *=8 tev data collected with the ATLAS detector*, ATLAS NOTE, 2013.

[Col13g] CMS Collaboration, *Search for invisible decays of a Higgs produced in association with a Z boson*, Tech. Rep. CMS-PAS-HIG-13-018 (2013).

[Col13h] FERMILAB Collaboration, *Higgs boson studies at the Tevatron*, arXiv:1303.6346v3 (2013).

[Cra] Kyle Cranmer, *Practical statistics for the LHC*.

[cswg11] LHC Higgs cross section working group, *Handbook of LHC Higgs cross sections: 1. inclusive observables*, arXiv:1101.0593 hep-ph. CERN-2011-002 (2011).

[cswg12] ———, *Handbook of LHC Higgs cross sections: 2. differential distributions*, arXiv:1201.3084 hep-ph. CERN-2012-002 (2012).

[cswg13] ———, *Handbook of LHC Higgs cross sections: 3. higgs properties*, arXiv:1307.1347v2 [hep-ph] (2013).

[Dan98] Reinier Josephus Dankers, *The physics performance of and level 2 trigger for the inner detector of ATLAS*, PhD thesis (1998).

[ea03a] John Rigden $etal$, *Building blocks of matter*, Macmillan Reference USA, 2003.

[ea03b] M.Mangano $etal$, *ALPGEN, a generator for hard multiparton processes in hadronic collision*, High Energy Phys. **07** (2003).

[ea04] T.Gleisberg $etal$, *Sherpa 1.alpha, a proof-of-concept version*, High Energy Phys. **02** (2004).

[ea09a] Kyle Cranmer $etal$, *Roostats users' guide v0*.

[ea09b] S. Alioli $etal$, *Nlo higgs boson production via gluon fusion matched with shower in POWHEG*, arXiv:0812.0578 hep-ph (2009).

[ea12] Kyle Cranmer $etal$, *Histfactory: A tool for creating statistical models for use with Roofit and Roostats*, CERN-OPEN-2012-016 (2012).

[EB08] L. Evans and P. Bryant, *LHC machine s08001*, JINST **3** (2008).

[Ege98] Ulrik Egede, *The search for a Standard Model Higgs at the LHC and electron identification using transition radiation in the ATLAS tracker*, Phd, Lund University, 1998.

[eta10] Glen Cowan etal, *Asymptotic formulae for likelihood-based tests of new physics*, arXiv:1007.1727v2 (2010).

[F.E64] R.Brout F.Englert, *Broken symmetry and the mass of gauge vector mesons*, Physical review Letters **13** (1964).

[ftAc08] H.J. Kim (for the ATLAS collaboration), *Electron and photon identification performance in ATLAS*, arXiv:0810.3415v1 hep-ex (2008).

[ftAc12] Marianna Testa (for the ATLAS collaboration), *Refined reconstruction and calibration of the missing transverse energy in the ATLAS detector*, arXiv:1201.4982v2 physics.ins.det (2012).

[Gri08] David Griffiths, *Introduction to elementary particles*, Wiley-VCH verlag GmbH and Co. KGaA Weinheim, 2008.

[JG62] Steven Weinberg Jefrey Goldstone, Abdus Salam, *Broken symmetries*, The Physical Review **127** (1962).

[L.R00] A L.Read, *Modified frequentist analysis of search results (the CLs method)*.

[Man10] Robert Mann, *Particle Physics and the Standard Model*, Taylor and Francis Group, 2010.

[MG08] G.P.Salam M.Cacciari and G.Soyez, *The anti-k_t jet clustering algorithm*, JHEP **04** (2008).

[M.K01] Sundaresan M.K, *Hand book of particle physics*, Boca Raton, 2001.

[MM02] Christopher G.Tully Marumi M.Kado, *The searches for Higgs bosons at LEP*, Anual Reviews (2002).

[Mos11] Nicolas Moser, *A sensitivity study for Higgs boson production in vector boson fusion in the H$\rightarrow \tau\tau \rightarrow lh + 3\nu$ final state with ATLAS*, PhD thesis, Universitt Bonn (2011).

[NO10] P. Nason and C. Oleari, *Nlo higgs boson production via vector-boson fusion matched with shower in POWHEG*, arXiv:0911.5299 hep-ph (2010).

[Sea03] LEP Working Group For Higgs Boson Searches, *Search for the Standard Model Higgs boson at LEP*, arXiv:0306033v1 [hep-ex] (2003).

[Std14] *Standard model*, http://en.wikipedia.org/wiki/Standard_Model#cite_note-1, Accessed March 2014.

[vE07] Niels van Eldik, *The ATLAS muon spectrometer: calibration and pattern recognition*, PhD thesis, Universitt Bonn (2007).

[Vir12] T.S Virdee, *Physics requirements for the design of ATLAS and CMS experiments at the Large Hadron Collider*, Royal Society Publishing (2012).

[W.H64] Peter W.Higgs, *Broken symmetries and the masses of gauge bosons*, Physical review Letters **13** (1964).

[WV08] D. Kirkby W. Verkerke, *Roofit users' manual v2.91*.

Appendix A.

Channel XML file For 7 TeV Signal Region one (SR1) at 125 GeV

```
<!DOCTYPE Channel  SYSTEM 'HistFactorySchema.dtd' >
<Channel Name="ATLAS_monojet_SR1_7TeV" InputFile="Histograms_SR1_7TeV.root"
<Data HistoName="nominal_Data_SR1_7TeV"/>
<StatErrorConfig RelErrorThreshold="0.0"    ConstraintType="Poisson" />

    <Sample Name="ggF_mH125_7TeV" HistoName="nominal_ggF_mH125_SR1_7TeV"
NormalizeByTheory="False" >
     <StatError Activate="False" />
      <OverallSys Name="QCDscale_ggFH1j"    Low="0.922"    High="1.071"/>
      <OverallSys Name="pdf_gg"     Low="0.929"     High="1.076"/>
      <OverallSys Name="HiggsPt_ggF"     Low="0.999"     High="1.001"/>
      <OverallSys Name="ATLASMC"     Low="0.97619"     High="1.02368"/>
      <OverallSys Name="ATLASJES"     Low="0.9655"     High="1.0321"/>
      <OverallSys Name="ATLASLEPEFF"     Low="0.992"     High="1.008"/>
      <OverallSys Name="ATLASLUMI"     Low="0.961"     High="1.039"/>
      <NormFactor Name="mu" Val="1"     Low="0."     High="15." Const="True"/
    </Sample>

    <Sample Name="VBF_mH125_7TeV" HistoName="nominal_VBF_mH125_SR1_7TeV"
NormalizeByTheory="False" >
     <StatError Activate="False" />
      <OverallSys Name="QCDscale_VBFH1j"     Low="0.997"     High="1.003"/>
      <OverallSys Name="pdf_qqbar"     Low="0.979"     High="1.025"/>
      <OverallSys Name="HiggsPt_VBF"     Low="0.9992"     High="1.0008"/>
      <OverallSys Name="ATLASMC"     Low="0.945785"     High="1.05259"/>
      <OverallSys Name="ATLAS_JES"     Low="0.961"     High="1.0396"/>
      <OverallSys Name="ATLAS_LEPEFF"     Low="0.992"     High="1.008"/>
      <OverallSys Name="ATLAS_LUMI"     Low="0.961"     High="1.039"/>
      <NormFactor Name="mu" Val="1"  Low="0."  High="15." Const="True"/>
    </Sample>
```

```
    <Sample Name="WH_mH125_7TeV" HistoName="nominal_WH_mH125_SR1_7TeV"
NormalizeByTheory="False" >
     <StatError Activate="False" />
      <OverallSys Name="QCDscale_VHH1j"      Low="0.991"    High="1.009"/>
      <OverallSys Name="pdf_qqbar"       Low="0.974"     High="1.026"/>
      <OverallSys Name="HiggsPt_VH"        Low="0.9988"    High="1.0012"/>
      <OverallSys Name="ATLAS_MC"       Low="0.899745"    High="1.09943"/>
      <OverallSys Name="ATLAS_JES"      Low="0.9624"    High="1.038"/>
      <OverallSys Name="ATLAS_LEPEFF"       Low="0.992"     High="1.008"/>
      <OverallSys Name="ATLAS_LUMI"       Low="0.961"     High="1.039"/>
      <NormFactor Name="mu" Val="1" Low="0." High="15." Const="True"/>
    </Sample>

    <Sample Name="ZH_mH125_7TeV" HistoName="nominal_ZH_mH125_SR1_7TeV"
NormalizeByTheory="False" >
     <StatError Activate="False" />
      <OverallSys Name="QCDscale_VHH1j"      Low="0.971"    High="1.029"/>
      <OverallSys Name="pdf_qqbar"       Low="0.973"     High="1.027"/>
      <OverallSys Name="HiggsPt_VH"      Low="0.9992"     High="1.0008"/>
      <OverallSys Name="ATLAS_MC"       Low="0.86865"     High="1.13051"/>
      <OverallSys Name="ATLAS_JES"      Low="0.9564"     High="1.0454"/>
      <OverallSys Name="ATLAS_LEPEFF"                Low="0.992"
High="1.008"/>
      <OverallSys Name="ATLAS_LUMI"      Low="0.961"     High="1.039"/>
      <NormFactor Name="mu" Val="1" Low="0." High="15." Const="True"/>
    </Sample>

    <Sample Name="Zvv_7TeV" HistoName="nominal_Zvv_SR1_7TeV"
NormalizeByTheory="False" >
     <StatError Activate="True" />
      <OverallSys Name="ATLAS_MC"       Low="0.995714"    High="1.00429"/>
      <OverallSys Name="ATLAS_JES"      Low="0.9845"     High="1.0155"/>
      <OverallSys Name="ATLAS_BKGSUB_Zvv"     Low="0.99"     High="1.01"/>
      <OverallSys Name="ATLAS_SHAP_Zvv"      Low="0.97"     High="1.03"/>
    </Sample>
```

```
    <Sample Name="Wtv_7TeV"  HistoName="nominal_Wtv_SR1_7TeV"
NormalizeByTheory="False" >
     <StatError Activate="True" />
      <OverallSys Name="ATLAS_MC"      Low="0.994936"     High="1.00506"/>
      <OverallSys Name="ATLAS_JES"      Low="0.9845"     High="1.0155"/>
      <OverallSys Name="ATLAS_BKGSUB"     Low="0.99"     High="1.01"/>
      <OverallSys Name="ATLAS_SHAP"      Low="0.97"     High="1.03"/>
    </Sample>

    <Sample Name="Wev_7TeV"      HistoName="nominal_Wev_SR1_7TeV"
NormalizeByTheory="False" >
     <StatError Activate="True" />
      <OverallSys Name="ATLAS_MC"      Low="0.993904"     High="1.0061"/>
      <OverallSys Name="ATLAS_JES"      Low="0.9845"     High="1.0155"/>
      <OverallSys Name="ATLAS_BKGSUB"     Low="0.99"     High="1.01"/>
      <OverallSys Name="ATLAS_SHAP"      Low="0.97"     High="1.03"/>
    </Sample>

    <Sample Name="Wmv_7TeV"  HistoName="nominal_Wmv_SR1_7TeV"
NormalizeByTheory="False" >
     <StatError Activate="True" />
      <OverallSys Name="ATLAS_MC"      Low="0.990901"     High="1.0091"/>
      <OverallSys Name="ATLAS_JES"      Low="0.9845"     High="1.0155"/>
      <OverallSys Name="ATLAS_BKGSUB"     Low="0.99"     High="1.01"/>
      <OverallSys Name="ATLAS_SHAP"      Low="0.97"     High="1.03"/>
    </Sample>

    <Sample Name="Ztt_7TeV"    HistoName="nominal_Ztt_SR1_7TeV"
NormalizeByTheory="False" >
     <StatError Activate="True" />
      <OverallSys Name="ATLAS_MC"      Low="0.976247"     High="1.02375"/>
      <OverallSys Name="ATLAS_JES"      Low="0.9845"     High="1.0155"/>
      <OverallSys Name="ATLAS_BKGSUB"     Low="0.99"     High="1.01"/>
      <OverallSys Name="ATLAS_SHAP"      Low="0.97"     High="1.03"/>
    </Sample>
```

```
    <Sample Name="Zmm_7TeV"        HistoName="nominal_Zmm_SR1_7TeV"
NormalizeByTheory="False" >
     <StatError Activate="True" />
      <OverallSys Name="ATLAS_MC"       Low="0.926471"      High="1.07353"/>
      <OverallSys Name="ATLAS_JES"      Low="0.9845"        High="1.0155"/>
      <OverallSys Name="ATLAS_BKGSUB"       Low="0.99"        High="1.01"/>
      <OverallSys Name="ATLAS_SHAP"       Low="0.97"        High="1.03"/>
    </Sample>

    <Sample Name="Multij_7TeV"   HistoName="nominal_Multij_SR1_7TeV"
NormalizeByTheory="False" >
     <StatError Activate="True" />
      <OverallSys Name="ATLAS_MC"      Low="1"       High="1"/>
      <OverallSys Name="ATLAS_JES"        Low="0.9845"      High="1.0155"/>
      <OverallSys Name="ATLAS_BKGSUB"      Low="0.99"        High="1.01"/>
      <OverallSys Name="ATLAS_SHAP"      Low="0.97"        High="1.03"/>
    </Sample>

    <Sample Name="ttbar_7TeV"   HistoName="nominal_ttbar_SR1_7TeV"
NormalizeByTheory="False" >
     <StatError Activate="True" />
      <OverallSys Name="ATLAS_MC"      Low="0.991129"      High="1.00887"/>
      <OverallSys Name="ATLAS_JES"       Low="0.9845"       High="1.0155"/>
      <OverallSys Name="ATLAS_LEPEFF"        Low="0.992"      High="1.008"/>
      <OverallSys Name="ATLAS_LUMI"        Low="0.961"      High="1.039"/>
    </Sample>

    <Sample Name="Dibo_7TeV"        HistoName="nominal_Dibo_SR1_7TeV"
NormalizeByTheory="False" >
      <OverallSys Name="ATLAS_MC"    Low="0.990066"      High="1.00993"/>
      <OverallSys Name="ATLAS_JES"      Low="0.9845"       High="1.0155"/>
      <OverallSys Name="ATLAS_LEPEFF"      Low="0.992"       High="1.008"/>
      <OverallSys Name="ATLAS_LUMI"        Low="0.961"       High="1.039"/>
    </Sample>

    <Sample Name="NonC_7TeV"                HistoName="nominal_NonC_SR1_7TeV"
NormalizeByTheory="False" >
```

```
      <OverallSys Name="ATLAS_MC"       Low="1"       High="1"/>
      <OverallSys Name="ATLAS_JES"      Low="0.9845"      High="1.0155"/>
      <OverallSys Name="ATLAS_BKGSUB"       Low="0.99"       High="1.01"/>
      <OverallSys Name="ATLAS_SHAP"      Low="0.97"      High="1.03"/>
    </Sample>
  </Channel>
```

Combination XML File For 7 TeV Signal Region one (SR1) at 125 GeV

```
<!DOCTYPE Combination  SYSTEM 'HistFactorySchema.dtd'>
<Combination OutputFilePrefix="hmonojet_125_sr1"  >
  <Input>hmonojetsr1_125_7TeV.xml</Input>
  <Measurement Name="allsys" Lumi="1" LumiRelErr="0.0001" BinLow="0"
   BinHigh="60" Mode="comb" ExportOnly="True">
    <POI>mu</POI>
  </Measurement>
</Combination>
```